118. Structural and Photophysical Properties of Pseudo-Tricapped Trigonal Prismatic Lanthanide Building Blocks Controlled by Zinc(II) in Heterodinuclear d–f Complexes

by **Claude Piguet*** and **Elisabeth Rivara-Minten**

Department of Inorganic, Analytical, and Applied Chemistry, University of Geneva, 30, quai Ernest-Ansermet, CH–1211 Genève 4

and **Gérard Hopfgartner**

F. Hoffmann-La Roche Ltd., Pharma Division, Department of Drug Metabolism and Kinetics, Bioanalytical Section, CH–4002 Basel

and **Jean-Claude G. Bünzli***

Institute of Inorganic and Analytical Chemistry, University of Lausanne, BCH 1402, CH–1015 Lausanne-Dorigny

(18.V.95)

An efficient combination of electrospray mass spectrometry (ES-MS), spectrophotometric and ^{1}H-NMR titrations in solution is used to characterize the assembly of the segmental ligand 2-{6-[1-(3,5-dimethoxybenzyl)-1*H*-benzimidazol-2-yl]pyridin-2-yl}-1,1′-dimethyl-5,5′-methylene-2′-(5-methylpyridin-2-yl)bis[1*H*-benzimidazole] ($\mathbf{L}^2$) with Zn^{II} and 4f metal ions, Ln^{III}. Ligand $\mathbf{L}^2$ reacts with $Zn(ClO_4)_2$ in MeCN to give successively $[Zn(\mathbf{L}^2)_2]^{2+}$, where the metal ion is coordinated by the tridentate binding units of the ligands, and the double-helical head-to-head complex $[Zn_2(\mathbf{L}^2)_2]^{4+}$. When $\mathbf{L}^2$ reacts with $Ln(ClO_4)_3$ (Ln = La, Eu, Lu), La^{III} only leads to a well-defined cylindrical C_1-symmetrical homodinuclear head-to-tail complex $[La_2(\mathbf{L}^2)_3]^{6+}$ in solution, while chemical-exchange processes prevent the ^{1}H-NMR characterization of $[Eu_2(\mathbf{L}^2)_3]^{6+}$, and Lu^{III} gives complicated mixtures of complexes. However, stoichiometric amounts of Ln^{III} (Ln = La, Ce, Pr, Nd, Sm, Eu, Tb, Y, Lu), Zn^{II}, and $\mathbf{L}^2$ in a 1:1:3 ratio lead to the selective formation of the C_3-symmetrical heterodinuclear complexes $[LnZn(\mathbf{L}^2)_3]^{5+}$ under thermodynamic control. Detailed NOE studies show that the ligands are wrapped about the C_3 axis defined by the metal ions, and the separation of dipolar and contact contributions to the ^{1}H-NMR paramagnetic shifts of the axial complexes $[LnZn(\mathbf{L}^2)_3]^{5+}$ (Ln = Ce, Pr, Nd, Sm, Eu) in MeCN establishes that Zn^{II} occupies the pseudo-octahedral capping coordination site defined by the three bidentate binding units, while Ln^{III} lies in the resulting 'facial' pseudo-tricapped trigonal prismatic site produced by the three remaining tridentate units. Photophysical measurements show that $[LnZn(\mathbf{L}^2)_3]^{5+}$ (Ln = Eu, Tb) are only weakly luminescent because of quenching processes associated with the C_3-cylindrical structure of the complexes. The use of 3d metal ions to control and design isomerically pure 'facial' tricapped trigonal prismatic lanthanide building blocks is discussed together with the calculation of a new nephelauxetic parameter associated with heterocyclic N-atoms coordinated to Ln^{III}.

Introduction. – The design of new supramolecular devices [1] for electron transfer [2], charge separation [3], and light conversion [4] is a subject of considerable current interest. In many cases, the planned device requires the preparation of organized heteropolynuclear complexes [3–5] which are prepared by the assembly of kinetically inert building blocks [3] [6] and/or by the selective complexation of the different metal ions with suitable coordinating units possessing various donor atoms [7]. However, the recent development of selective self-assembly processes between segmental ligands and metal ions leading to programmed architectures [8] [9] has reached a point where it is now possible to tailor

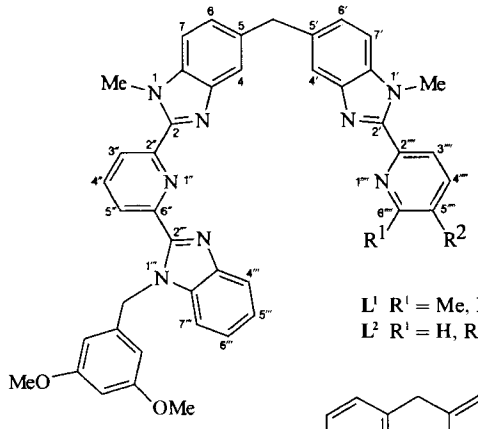

L^1 $R^1 = Me$, $R^2 = H$
L^2 $R^1 = H$, $R^2 = Me$

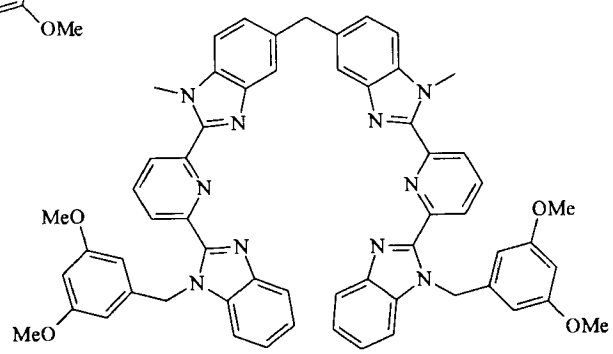

L^3

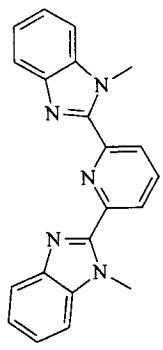

L^4

oligo-multidentate receptors with similar coordinating units, but which are able to recognize different metal ions [10–13]. *E.g.*, similar oligo-bipyridines differing only in the position of the spacers connecting the bidentate binding units lead to the quantitative separation of double helicates with Cu^I and triple helicates with Ni^{II} from a mixture of ligands and metal ions [10], while segmental ligands with coordinating units which differ only in their denticity [11] allow the selective complexation of Ag^I and Fe^{II} in organometallic heterotrinuclear [2]catenates [12]. Recently, we showed that $\mathbf{L}^1$ reacts with Fe^{II} and Ag^I to give the heterodinuclear double helix $[FeAg(\mathbf{L}^1)_2]^{3+}$ [13]. If the Me group bound to C(6'''') of the pyridine ring in $\mathbf{L}^1$ is shifted to C(5''''), the resulting ligand $\mathbf{L}^2$ possesses a bidentate binding unit more suitable for pseudo-octahedral coordination of d-block metal ions [14] and is a good candidate for the simultaneous complexation of 3d and 4f metal ions. This new approach offers promising possibilities for the preparation of heterodinuclear d–f complexes with controlled coordination spheres, and we recently reported the isolation and characterization of the first heterodinuclear d–f triple-helical complex $[LaZn(\mathbf{L}^2)_3]^{5+}$ in a preliminary communication [15]. This paper describes the preparation and structural characterization of the heterodinuclear complexes $[LnZn(\mathbf{L}^2)_3]^{5+}$ (Ln = La-Lu) in solution. It also presents a detailed study of the thermodynamic assembly processes which control the formation of the homo- and heterodinuclear complexes of $\mathbf{L}^2$ with Zn^{II} and Ln^{III}, as well as their photophysical properties in the solid state.

Results and Discussion. – *Preliminary Remarks.* The ligand $\mathbf{L}^2$ possesses two different binding units separated by a 'diphenylmethane' spacer which favors the formation of helical complexes [9] [13]. The tridentate unit, an analogue of 2,2′:6′,2″-terpyridine [16], is suitable for the pseudo-tricapped trigonal prismatic coordination of lanthanides [5] [17], while the bidentate unit allows the efficient pseudo-octahedral coordination of 3d metal ions [14]. We thus expect that $\mathbf{L}^2$ will react with an equimolar mixture of 3d and 4f metal ions to produce cylindrical heterodinuclear d–f complexes. To investigate these assembly processes in solution, we used electrospray mass spectrometry (ES-MS) for the qualitative speciation [18–20], combined with spectrophotometric titrations for the quantitative speciation [9] [13] and ^{1}H-NMR techniques for the structural investigation [12] [13]. The fully characterized complexes were then isolated as their perchlorate salts under controlled concentration and solvent conditions.

Homodinuclear Complexes of $\mathbf{L}^2$ *with* Zn^{II}. ES-MS Titrations of $\mathbf{L}^2$ with $Zn(ClO_4)_2 \cdot 6\,H_2O$ in MeCN show the successive formation of two major species $[Zn(\mathbf{L}^2)_2]^{2+}$ (*m/z* 743.2) and $[Zn_2(\mathbf{L}^2)_2]^{4+}$ (*m/z* 388, *Table 1*). In presence of an excess of ligand ($Zn/\mathbf{L}^2 = 0.3$), traces of $[Zn(\mathbf{L}^2)_3]^{2+}$ are observed together with a strong peak corresponding to the free ligand $[\mathbf{L}^2 + H]^+$ (*m/z* 711.8). Upon complexation to Zn^{2+}, the $\pi \rightarrow \pi^*$ transition centered at 31450 cm^{-1} for $\mathbf{L}^2$ is split into two major components resulting from the coordination of the tridentate unit to the metal ion which strongly affects the energy of the π^* and π orbitals of the ligand [17], as previously described for $[Zn(\mathbf{L}^1)_2]^{2+}$ and $[Zn_2(\mathbf{L}^1)_2]^{4+}$ [13] and for complexes with the tridentate ligand $\mathbf{L}^4$: $[M(\mathbf{L}^4)_2]^{2+}$ (M = Zn, Cu [21]; M = Fe [16]) and $[Ln(\mathbf{L}^4)_3]^{3+}$ (Ln = La, Eu, Gd, Tb) [17] (*Table 2*). These variations of the UV spectra are monitored spectrophotometrically for $Zn/\mathbf{L}^2$ ratios in the range 0.1–2.0, and we observe two sharp end points for metal/ligand ratios of 0.5 and 1.0, in agreement with

Table 1. *Molecular Peaks of Complexes of* $\mathbf{L}^2$ *and Adduct Ions Observed by ES-MS*

Metal	Cation	*m/z*[a])	Metal	Cation	*m/z*[a])
Zn^{II}	$[Zn(\mathbf{L}^2)_3]^{2+}$	1098.2	Eu^{III}/Zn^{II}	$[EuZn(\mathbf{L}^2)_3]^{5+}$	469.8
	$[Zn(\mathbf{L}^2)_2]^{2+}$	743.2		$[EuZn(\mathbf{L}^2)_3(ClO_4)]^{4+}$	612.0
	$[Zn_2(\mathbf{L}^2)_2]^{4+}$	388.0		$[EuZn(\mathbf{L}^2)_3(ClO_4)_2]^{3+}$	849.4
	$[Zn_2(\mathbf{L}^2)_2(ClO_4)]^{3+}$	550.8		$[EuZn(\mathbf{L}^2)_3(ClO_4)_3]^{2+}$	1323.8
La^{III}	$[La_2(\mathbf{L}^2)_3(ClO_4)]^{5+}$	501.8		$[Zn(\mathbf{L}^2)_2]^{2+}$	743.6
	$[La_2(\mathbf{L}^2)_3(ClO_4)_2]^{4+}$	652.1	Tb^{III}/Zn^{II}	$[TbZn(\mathbf{L}^2)_3]^{5+}$	471.2
	$[La_2(\mathbf{L}^2)_3(ClO_4)_3]^{3+}$	902.6		$[TbZn(\mathbf{L}^2)_3(ClO_4)]^{4+}$	614.0
Eu^{III}	$[Eu_2(\mathbf{L}^2)_3(ClO_4)]^{5+}$	507.2		$[TbZn(\mathbf{L}^2)_3(ClO_4)_2]^{3+}$	851.8
	$[Eu_2(\mathbf{L}^2)_3(ClO_4)_2]^{4+}$	658.6		$[TbZn(\mathbf{L}^2)_3(ClO_4)_3]^{2+}$	1327.2
	$[Eu_2(\mathbf{L}^2)_3(ClO_4)_3]^{3+}$	911.4		$[Zn(\mathbf{L}^2)_2]^{2+}$	743.0
La^{III}/Zn^{II}	$[LaZn(\mathbf{L}^2)_3]^{5+}$	467.3	Y^{III}/Zn^{II}	$[YZn(\mathbf{L}^2)_3]^{5+}$	457.2
	$[LaZn(\mathbf{L}^2)_3(ClO_4)]^{4+}$	608.8		$[YZn(\mathbf{L}^2)_3(ClO_4)]^{4+}$	596.5
	$[LaZn(\mathbf{L}^2)_3(ClO_4)_2]^{3+}$	845.0		$[YZn(\mathbf{L}^2)_3(ClO_4)_2]^{3+}$	828.2
	$[LaZn(\mathbf{L}^2)_3(ClO_4)_3]^{2+}$	1317.5		$[YZn(\mathbf{L}^2)_3(ClO_4)_3]^{2+}$	1292.6
	$[Zn(\mathbf{L}^2)_2]^{2+}$	742.9		$[Zn(\mathbf{L}^2)_2]^{2+}$	743.2
Nd^{III}/Zn^{II}	$[NdZn(\mathbf{L}^2)_3]^{5+}$	468.3	Lu^{III}/Zn^{II}	$[LuZn(\mathbf{L}^2)_3]^{5+}$	474.5
	$[NdZn(\mathbf{L}^2)_3(ClO_4)]^{4+}$	610.0		$[LuZn(\mathbf{L}^2)_3(ClO_4)]^{4+}$	618.0
	$[NdZn(\mathbf{L}^2)_3(ClO_4)_2]^{3+}$	846.8		$[LuZn(\mathbf{L}^2)_3(ClO_4)_2]^{3+}$	857.0
	$[NdZn(\mathbf{L}^2)_3(ClO_4)_3]^{2+}$	1320.0		$[LuZn(\mathbf{L}^2)_3(ClO_4)_3]^{2+}$	1335.5
	$[Zn(\mathbf{L}^2)_2]^{2+}$	743.0		$[Zn(\mathbf{L}^2)_2]^{2+}$	743.2

[a]) *m/z* Values given for the maximum of the peak.

Table 2. *Electronic Spectral Data for the Ligand* L^2 *in* $CHCl_3$ *and Its Complexes in MeCN at 293 K*[a])

	$\pi_{dmb} \rightarrow \pi^*$[b])	$\pi \rightarrow \pi^*$		$\pi_{dmb} \rightarrow \pi^*$[b])	$\pi \rightarrow \pi^*$
L^2	35490(sh, 28500)	31450(55630)	$[NdZn(L^2)_3]^{5+}$	35260(sh, 58390)	31150(96580)
$[Zn(L^2)_2]^{2+}$	35715(sh, 49930)	31850(94000)			29240(sh, 70640)
		27780(sh, 41120)			27030(47340)
$[Zn_2(L^2)_2]^{4+}$	35715(sh, 41990)	31645(89010)	$[SmZn(L^2)_3]^{5+}$	35210(sh, 59500)	31970(97700)
		28900(77310)			29240(sh, 72200)
		27400(sh, 41500)			26940(48200)
$[La_2(L^2)_3]^{6+}$	35715(sh, 49270)	31645(77550)	$[EuZn(L^2)_3]^{5+}$	35210(sh, 57800)	31350(94800)
		28410(sh, 66340)			29310(sh, 71200)
		26810(sh, 45090)			27030(47300)
$[LaZn(L^2)_3]^{5+}$	35751(sh, 56880)	31545(99850)	$[TbZn(L^2)_3]^{5+}$	35210(sh, 57940)	31400(95100)
		28985(sh, 68980)			29250(sh, 70800)
		27400(46980)			27010(47800)
$[CeZn(L^2)_3]^{5+}$	35210(sh, 59410)	31020(96630)	$[YZn(L^2)_3]^{5+}$	35250(sh, 59000)	31120(96020)
		29070(sh, 67830)			29300(sh, 71400)
		27100(47640)			27030(48000)
$[PrZn(L^2)_3]^{5+}$	35460(sh, 57930)	31060(96900)	$[LuZn(L^2)_3]^{5+}$	35210(sh, 58500)	31060(95200)
		29240(sh, 71910)			29240(sh, 70600)
		27030(48490)			27010(47500)

[a]) Energies are given for the maximum of the band envelope in cm^{-1} and ε (in parentheses) in $M^{-1} \cdot cm^{-1}$; sh = shoulder.

[b]) Transitions centered on the 3,5-dimethoxyphenyl rings [16] [17].

ES-MS titrations under the same conditions. Factor analysis [22] suggests the existence of only two different absorbing complexes, and the spectrophotometric data can be satisfactorily fitted with the equilibria of *Eqns. 1* and *2*.

$$Zn^{2+} + 2\,L^2 \rightleftarrows [Zn(L^2)_2]^{2+} \quad \log(\beta_{12}^{Zn}) = 15.4(8) \tag{1}$$

$$2\,Zn^{2+} + 2\,L^2 \rightleftarrows [Zn_2(L^2)_2]^{4+} \quad \log(\beta_{22}^{Zn}) = 22(1) \tag{2}$$

Table 3. *^{1}H-NMR Shifts* (rel. to $SiMe_4$) *for Ligand* L^2

	Bidentate binding unit								
	Me–C(5‴)	Me–N(1′)	H–C(6‴)	H–C(4‴)	H–C(3‴)	H–C(7′)	H–C(6′)	H–C(4′)	CH_2–C(5′)
L^2	2.39	4.21	8.49	7.61	8.22	7.30	7.18	7.66	4.26
$[Zn(L^2)_2]^{2+}$	2.46	4.27	8.61	7.78	8.27	7.25	6.81	7.13	3.80, 3.92
$[Zn_2(L^2)_2]^{4+}$	2.06	4.46	7.48	7.78	8.23	7.88	7.46	7.39	3.76, 4.08
$[La_2(L^2)_3]^{6+}$	2.01	4.18	8.10	7.82	8.17	7.25	7.20	5.87	2.96, 2.95
	1.95	3.63	8.06	7.40	7.49	7.36	7.08	6.06	3.50, 3.54
	1.90	3.48	7.90	7.48	7.37	7.50	6.80	6.02	3.18, 3.35
$[LaZn(L^2)_3]^{5+}$	2.13	4.03	7.90	7.80	8.13	7.22	6.87	5.18	3.22, 3.65
$[YZn(L^2)_3]^{5+}$	2.15	4.07	7.88	7.80	8.13	7.27	6.92	5.06	3.26, 3.62
$[LuZn(L^2)_3]^{5+}$	2.16	4.09	7.86	7.80	8.13	7.29	6.93	5.02	3.27, 3.59
$[CeZn(L^2)_3]^{5+}$	1.93	3.73	7.53	7.59	7.79	6.94	6.69	3.49	3.12, 3.30
$[PrZn(L^2)_3]^{5+}$	1.67	3.35	7.05	7.31	7.38	6.55	6.46	1.48	2.85, 3.03
$[NdZn(L^2)_3]^{5+}$	1.85	3.62	7.38	7.51	7.68	6.83	6.62	2.88	3.02, 3.15
$[SmZn(L^2)_3]^{5+}$	2.09	3.99	7.83	7.79	8.07	7.18	6.87	4.75	3.25, 3.58
$[EuZn(L^2)_3]^{5+}$	2.41	4.41	8.44	8.14	8.59	7.71	7.21	7.31	3.57, 4.17

These results parallel those obtained for the analogous ligand $\mathbf{L}^1$ where similar complexes were observed: $[Zn(\mathbf{L}^1)_2]^{2+}$ ($\log(\beta_{12}^{Zn}) = 14.3(8)$) and $[Zn_2(\mathbf{L}^1)_2]^{4+}$ ($\log(\beta_{22}^{Zn}) = 20.3(8)$) [13]. The ^{1}H-NMR spectrum of the free ligand $\mathbf{L}^2$ is rather complicated, but complete assignment of the 24 signals was performed using 2D-COSY and 2D-NOESY correlation spectroscopies and NOEDIF measurements (*Table 3*). Significant NOE's for H–C(6‴)/Me–N(1′) and CH_2–N(1″)/Me–N(1) together with no observable NOE's for H–C(3‴)/Me–N(1′), H–C(3″)/Me–N(1), and H–C(5″)/CH_2–N(1‴) imply that the pyridine and benzimidazole rings adopt '*transoïd*' (s-*trans*, *i.e.*, N(1″) *trans* to N(3) and N(3‴) and N(1⁗) *trans* to N(3′)) conformations within each coordinating unit as reported for $\mathbf{L}^1$ [13] and other oligopyridines [23]. According to *Eqns. 1* and *2*, we expect that the titration of $\mathbf{L}^2$ with Zn^{II} in MeCN at concentrations compatible with ^{1}H-NMR studies (*ca.* 0.01M) leads to the quantitative formation (> 95%) of $[Zn(\mathbf{L}^2)_2]^{2+}$ and $[Zn_2(\mathbf{L}^2)_2]^{4+}$ for metal/ligand ratios of 0.5 and 1.0, respectively. We indeed observe only 26 signals for a Zn/$\mathbf{L}^2$ ratio of 0.5 corresponding to the C_2-symmetrical complex $[Zn(\mathbf{L}^2)_2]^{2+}$ in solution [13]. Strong NOE's for Me–N(1)/H–C(3″) and CH_2–N(1‴)/H–C(5″) and the downfield shift of H–C(4″) (0.36 ppm) associated with N-coordination of the pyridine ring show that the tridentate binding unit of $\mathbf{L}^2$ adopts a *s-cis*/*s-cis* conformation typical of its coordination to the metal ion [13] [24]. The significant upfield shifts of H–C(4) and H–C(4‴) (1.83 and 1.62 ppm, resp.) result from a perpendicular arrangement of the tridentate units coordinated to Zn^{II} [16] and leading to the C_2-symmetrical head-to-head structure **I** for $[Zn(\mathbf{L}^2)_2]^{2+}$ (*Fig. 1*), as similarly reported for $[Zn(\mathbf{L}^1)_2]^{2+}$ [13]. These observations indicate that Zn^{II} displays a stronger affinity for the tridentate coordinating units of $\mathbf{L}^1$ and $\mathbf{L}^2$ even though the bidentate unit is less constrained in $\mathbf{L}^2$ and is more suitable for pseudo-octahedral coordination of 3d metal ions [14]. The addition of a second equiv. of Zn^{II} transforms quantitatively $[Zn(\mathbf{L}^2)_2]^{2+}$ into $[Zn_2(\mathbf{L}^2)_2]^{4+}$ and leads to 26 other ^{1}H-NMR signals corresponding to a C_2-symmetrical arrangement of the two ligands around the metal ions. The chemical shifts of the protons of the bidentate binding units are strongly affected, while those of the tridentate units are not significantly modified (*Table 3*). A

in $CDCl_3$ and Its Complexes in CD_3CN at 294 K

Tridentate binding unit											
Me–N(1)	H–C(4)	H–C(6)	H–C(7)	H–C(3″)	H–C(4″)	H–C(5″)	CH_2–N(1‴)	H–C(7‴)	H–C(6‴)	H–C(5‴)	H–C(4‴)
3.66	7.69	7.22	7.22	8.29	8.00	8.42	5.90	7.30	7.40	7.20	7.85
4.11	5.86	7.25	7.40	8.24	8.36	8.16	5.80, 5.84	7.41	7.23	6.95	6.23
4.13	5.87	7.21	7.40	8.41	8.36	8.13	5.84, 5.94	7.53	7.32	7.08	6.52
3.66	5.77	7.45	7.64	7.78	7.94	7.27	4.90, 5.44	7.31	7.22	6.80	6.70
4.16	5.88	7.29	7.19	8.41	8.09	7.25	4.42, 5.30	7.30	7.20	6.83	6.91
4.15	5.89	7.38	7.35	8.37	8.09	7.20	4.67, 5.30	7.40	7.15	6.59	6.71
3.94	5.92	7.29	7.69	7.89	7.88	7.30	4.78, 5.53	7.48	7.27	6.73	7.20
4.06	5.53	7.22	7.67	7.86	7.70	7.18	5.07, 5.75	7.43	7.24	6.76	6.83
4.09	5.42	7.20	7.66	7.86	7.66	7.16	5.16, 5.78	7.44	7.22	6.78	6.72
5.01	0.95	7.19	8.23	9.42	9.20	8.79	6.32, 6.84	8.24	7.44	6.41	3.18
6.37	–4.85	7.11	8.98	11.71	10.69	11.04	8.22, 8.57	9.21	7.62	5.96	–1.80
5.48	–0.65	7.15	8.85	11.00	9.89	10.34	6.96, 7.72	8.88	7.44	6.22	1.65
4.26	4.53	7.24	7.73	8.13	7.97	7.51	5.35, 5.92	7.58	7.30	6.67	6.01
2.65	11.55	7.37	5.93	3.53	5.29	2.94	3.04, 3.16	5.57	7.19	7.34	12.36

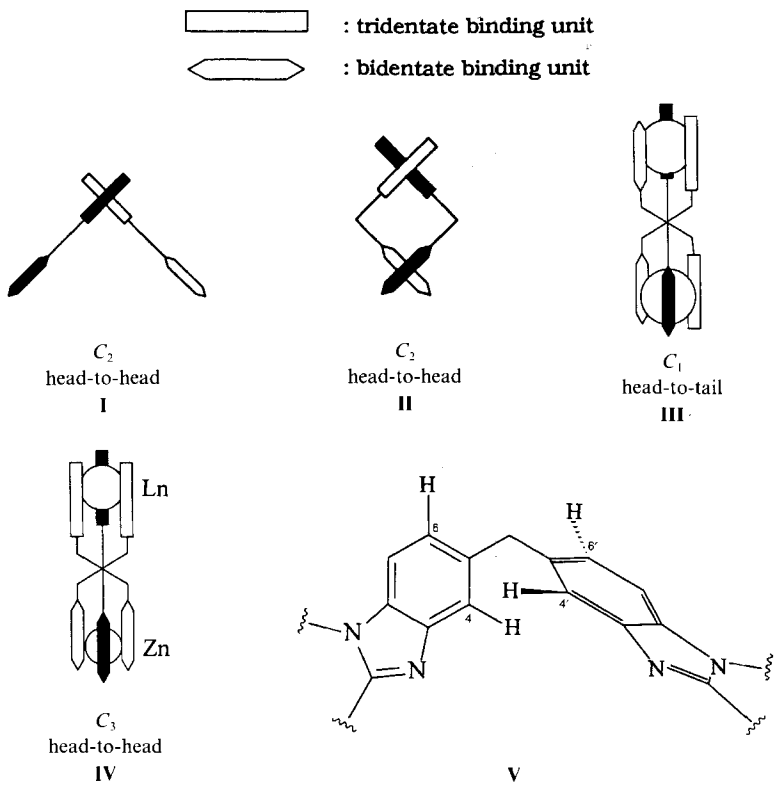

Fig. 1. *Different orientations of the bidentate and tridentate binding units* (see **I**–**IV**) *and 'diphenylmethane' spacer conformation* **V**

strong NOE for Me–N(1′)/H–C(3‴″) reveals that the bidentate units adopt a '*cisoïd*' (s-*cis*; *i.e.*, N(1‴″) *cis* to N(3′)) conformation, in agreement with its coordination to Zn^{II}. Detailed studies of the NOE's experienced by the protons situated near the spacer (H–C(4′),H–C(6′),H–C(4), and H–C(6)) parallel those found for $[Zn_2(\mathbf{L}^1)_2]^{4+}$ and show that the aromatic benzo moieties of the 'diphenylmethane' spacer adopt the conformation expected for a double-helical complex [13]. Finally, the large upfield shifts exhibited by H–C(6‴″) (1.13 ppm) and Me–C(5‴″) (0.4 ppm) when going from $[Zn(\mathbf{L}^2)_2]^{2+}$ to $[Zn_2(\mathbf{L}^2)_2]^{4+}$ indicate a pseudo-tetrahedral arrangement of the bidentate units around Zn^{II} which brings H–C(6‴″) of one pyridine ring in the shielding region of the second bidentate unit as similarly reported for pseudo-tetrahedral Cu^{I} complexes [9] and for the Me group bound to the pyridine ring in $[Zn_2(\mathbf{L}^1)_2]^{4+}$ [13]. We conclude that $[Zn_2(\mathbf{L}^2)_2]^{4+}$ adopts the C_2-symmetrical head-to-head double-helical structure **II** found for the analogous complex $[Zn_2(\mathbf{L}^1)_2]^{4+}$ (*Fig. 1*) [13]. This complex was isolated as its perchlorate salt by diffusion of MeOH into a MeCN solution to give pale-yellow crystals whose elemental analyses and IR spectra correspond to $[Zn_2(\mathbf{L}^2)_2](ClO_4)_4 \cdot 4\ H_2O$ (**1**). The compound is readily soluble in MeCN and gives ES-MS, ^{1}H-NMR, and UV/VIS spectra identical to those measured for the complex $[Zn_2(\mathbf{L}^2)_2]^{4+}$ prepared *in situ*, but we were unable to obtain crystals suitable for X-ray diffraction studies.

Homodinuclear Complexes of $\mathbf{L}^2$ *with* Ln^{III}. While the tridentate binding unit of $\mathbf{L}^2$ is suitable for coordination of Ln^{III} [5] [17], the bidentate unit displays only low affinities for these ions [25]. We thus expect the formation of intricate mixtures when $\mathbf{L}^2$ reacts with Ln^{III} [9]. Surprisingly, spectrophotometric titrations of $\mathbf{L}^2$ with $La(ClO_4)_3 \cdot 7\ H_2O$ for $La^{III}/\mathbf{L}^2$ ratios in the range 0.1–2.0 show a monotonic evolution with only one sharp end point for $La^{III}/\mathbf{L}^2 = 0.65$ (*Fig. 2a*). Factor analysis [22] confirms the existence of only two

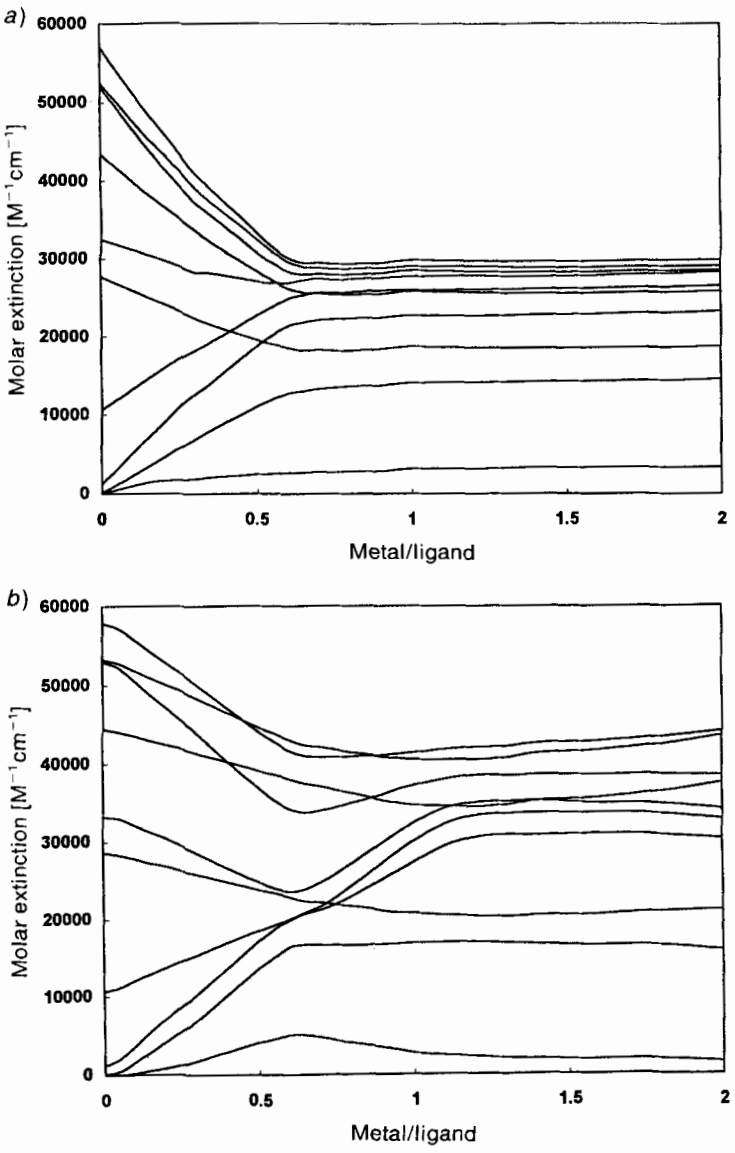

Fig. 2. *Variation of observed molar extinctions at 10 different wavelengths for the spectrophotometric titrations of* $\mathbf{L}^2$ *with* a) $La(ClO_4)_3 \cdot 7\ H_2O$ *and* b) $Lu(ClO_4)_3 \cdot 7.2\ H_2O$ *in MeCN at 293 K.* Total ligand concentration 10^{-4} M.

absorbing species, and the data can be satisfactorily fitted to the equilibrium of *Eqn. 3* (convergence is obtained with a root-mean-square (r.m.s.) difference between observed and calculated absorbance of 0.06 unit).

$$2\ La^{3+} + 3\ \mathbf{L}^2 \rightleftarrows [La_2(\mathbf{L}^2)_3]^{6+} \quad \log(\beta_{23}^{La}) = 22.3(3) \tag{3}$$

A similar behavior is observed for Ln = Eu, leading to the formation of $[Eu_2(\mathbf{L}^2)_3]^{6+}$ with $\log(\beta_{23}^{Eu}) = 23.5(8)$ and r.m.s. = 0.009. The ES-MS confirm the spectrophotometric results: the only significant peaks correspond to the free ligand ($[\mathbf{L}^2 + H]^+$, *m/z* 711.2; $[\mathbf{L}^2 + 2H]^{2+}$, *m/z* 356.3) and to the homodinuclear complex $[La_2(\mathbf{L}^2)_3]^{6+}$ ($[La_2(\mathbf{L}^2)_3(ClO_4)_i]^{(6-i)+}$, $i = 1$–3, *Table 1*) [19]. Because of the weak ES-MS response of these complexes, the observation of the molecular peaks and their adducts with perchlorate anions [18] [19] is critical and strongly depends on experimental conditions. The best results are obtained with MeCN solutions dried with 4 Å molecular sieves and using silica sprayers coated with hydrophobic polymers. ^{1}H-NMR Titration of $\mathbf{L}^2$ by $La(ClO_4)_3 \cdot 7\ H_2O$ at high total ligand concentration ($1.3 \cdot 10^{-2}$ M) shows the expected quantitative formation of $[La_2(\mathbf{L}^2)_3]^{6+}$ (*Eqn. 3*) which displays 78 signals in the ^{1}H-NMR spectrum (*Fig. 3a*). Detailed 2D-COSY (*Fig. 3b*) and NOEDIF experiments allow the complete assignment of the signals corresponding to three nonequivalent ligands and point to C_1 symmetry for $[La_2(\mathbf{L}^2)_3]^{6+}$ in MeCN (*Table 3*). The observation of NOE's for Me–N(1′)/H–C(3‴), Me–N(1)/H–C(3″), and CH_2–N(1‴)/H–C(5″) clearly establishes *s-cis* conformations within both the tridentate and bidentate binding units of the three ligands, consistent with their coordination to the metal ions [13]. The upfield shift of H–C(4′) and H–C(4) (1.7 and 1.9 ppm, resp.; 1.80 ppm for $[La_2(\mathbf{L}^3)_3]^{6+}$ [5]) is of particular interest, since it is associated with a conformation of the 'diphenylmethane' spacer characteristic of helical complexes. In the latter, H–C(4′) and H–C(4) lie above the plane of the second benzo moiety (structure **V**, *Fig. 1*), as observed in the crystal structure of $[Eu_2(\mathbf{L}^3)_3](ClO_4)_6$ [5] [26]. This suggests that $[La_2(\mathbf{L}^2)_3]^{6+}$ possesses the C_1-helical structure **III** where two ligands $\mathbf{L}^2$ adopt a head-to-head arrangement while the third ligand is oriented head-to-tail, leading to different environments around the metal ions with respectively seven and eight coordinated donor N-atoms. Solvent molecules are expected to complete the La^{III} coordination sphere in solution [27], even though solvated species were not detected by ES-MS.

When La^{III} is replaced by Eu^{III}, the ^{1}H-NMR spectrum still shows the formation of only one complex $[Eu_2(\mathbf{L}^2)_3]^{6+}$, but the broader signals prevent a detailed assignment. Since Eu^{III} exhibits the shortest relaxation time among the paramagnetic lanthanide ions [28] [29] and since well-resolved spectra are obtained for $[EuZn(\mathbf{L}^2)_3]^{5+}$ (*vide infra*), the broadening of the signals observed for $[Eu_2(\mathbf{L}^2)_3]^{6+}$ is tentatively attributed to chemical-exchange processes in solution. Titration of $\mathbf{L}^2$ with $Lu(ClO_4)_3 \cdot 7.2\ H_2O$ results in a complicated variation of the absorbance (*Fig. 2b*) with poorly defined end points. Factor analysis [22] suggests the formation of four absorbing species, but we were unable to fit the spectrophotometric data with reasonable models. ES-MS recorded under the same experimental conditions are dominated by the peaks of the free ligand, but minor signals may be tentatively attributed to $[Lu(\mathbf{L}^2)_2(ClO_4)_i]^{(3-i)+}$ (*m/z* 532.2 and 848.1 for $i = 1$ and 2, resp.) and $[Lu_2(\mathbf{L}^2)_2(ClO_4)_4]^{2+}$ (*m/z* 1085). As expected, ^{1}H-NMR titrations reveal a complicated evolution of the spectra and the presence of significant quantities of the free

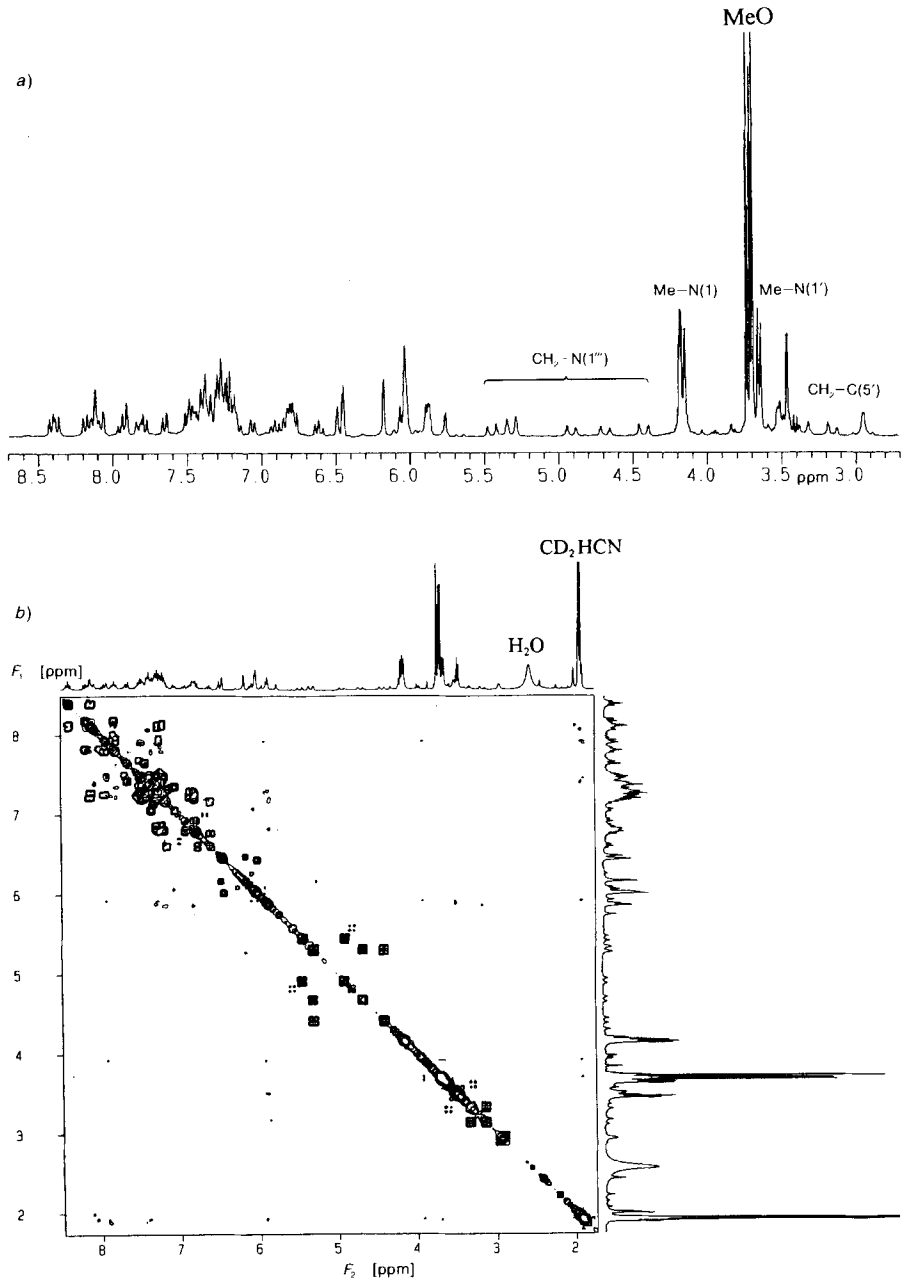

Fig. 3. a) *^{1}H-NMR Spectrum and* b) *2D-COSY correlation spectrum of* $[La_2(L^2)_3]^{6+}$ *in* CD_3CN *at 294 K.* Total ligand concentration $1.5 \cdot 10^{-2}$ M.

ligand L^2 for Lu/L^2 ratios in the range 0.1–2.0, suggesting the formation of intricate mixtures of unstable complexes in MeCN. Such features typically occur when the stereochemical requirements of the metal ion do not match the ligand-binding capabilities [9], and this system was not further investigated.

Therefore, it appears that the unexpected selective assembly of $[Ln_2(L^2)_3]^{6+}$ is limited to the larger lanthanide ions. This behavior strongly contrasts with that observed for the self-assembled triple-helical complexes $[Ln_2(L^3)_3]^{6+}$ which are stable in solution for the entire Ln series [5], and it is the consequence of the replacement of one tridentate unit in L^3 by a bidentate binding unit in L^2 having only weak affinity for Ln^{III} ions [25]. Perchlorate salts of $[Ln_2(L^2)_3]^{6+}$ (Ln = La, Eu) are difficult to isolate as pure compounds, and slow diffusion of solvents (Et_2O, MeOH, $MeNO_2$) into a MeCN solution of the complexes leads to partial decomplexation. However, evaporation of MeCN followed by treatment with EtOH affords analytically pure powders the elemental analyses of which correspond to $[La_2(L^2)_3](ClO_4)_6 \cdot EtOH \cdot 6\ H_2O$ (**2**) and $[Eu_2(L^2)_3](ClO_4)_6 \cdot EtOH \cdot 11\ H_2O$ (**3**). These compounds are readily soluble in MeCN and give spectra (ES-MS, UV/VIS, ^{1}H-NMR) identical to those obtained for the complexes prepared *in situ*.

Heterodinuclear Complexes of L^2 *with* Zn^{II} *and* Ln^{III}. Spectrophotometric titrations of L^2 by an equimolar mixture of $La(ClO_4)_3 \cdot 7\ H_2O$ and $Zn(ClO_4)_2 \cdot 6\ H_2O$ in the range metal/L^2 = 0.1–2.5 (metal = conc. La^{III} = conc. Zn^{II} with $L^2_{tot} = 10^{-4}$ M) show a complicated variation of molar extinctions with two end points at metal/L^2 = 0.3 and 1.0. A fit with *Eqns. 1–4* readily converges (r.m.s. = 0.002), suggesting that only one heterodinuclear complex $[LaZn(L^2)_3]^{5+}$ is formed during the titration.

$$La^{3+} + Zn^{2+} + 3\ L^2 \rightleftarrows [LaZn(L^2)_3]^{5+} \quad \log(\beta_{113}^{LaZn}) = 26.2(3) \tag{4}$$

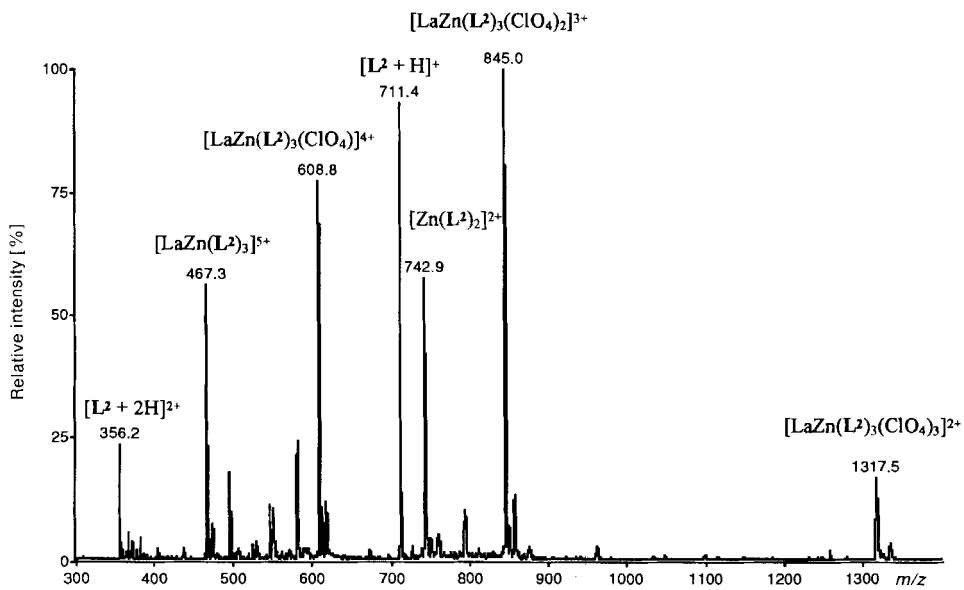

Fig. 4. *ES-MS of* $[LaZn(L^2)_3](ClO_4)_5 \cdot 5\ H_2O$ (**4**) *in MeCN*. Total ligand concentration $2 \cdot 10^{-4}$ M.

ES-MS under similar conditions ($L^2_{tot} = 2 \cdot 10^{-4}$ M, La/Zn/L^2 1:1:3) confirms this conclusion: the observed species are $[LaZn(L^2)_3]^{5+}$ (m/z 467.3), $[LaZn(L^2)_3(ClO_4)_i]^{(5-i)+}$ (i = 1–3, *Table 1*) and a significant peak attributed to $[Zn(L^2)_2]^{2+}$ (*Fig. 4*). These observations qualitatively agree with the distribution of species calculated from *Eqns. 1–4* which predicts comparable quantities of $[Zn(L^2)_2]^{2+}$ and $[LaZn(L^2)_3]^{5+}$ ($L^2_{tot} = 10^{-4}$ M, *Fig. 5a*). No

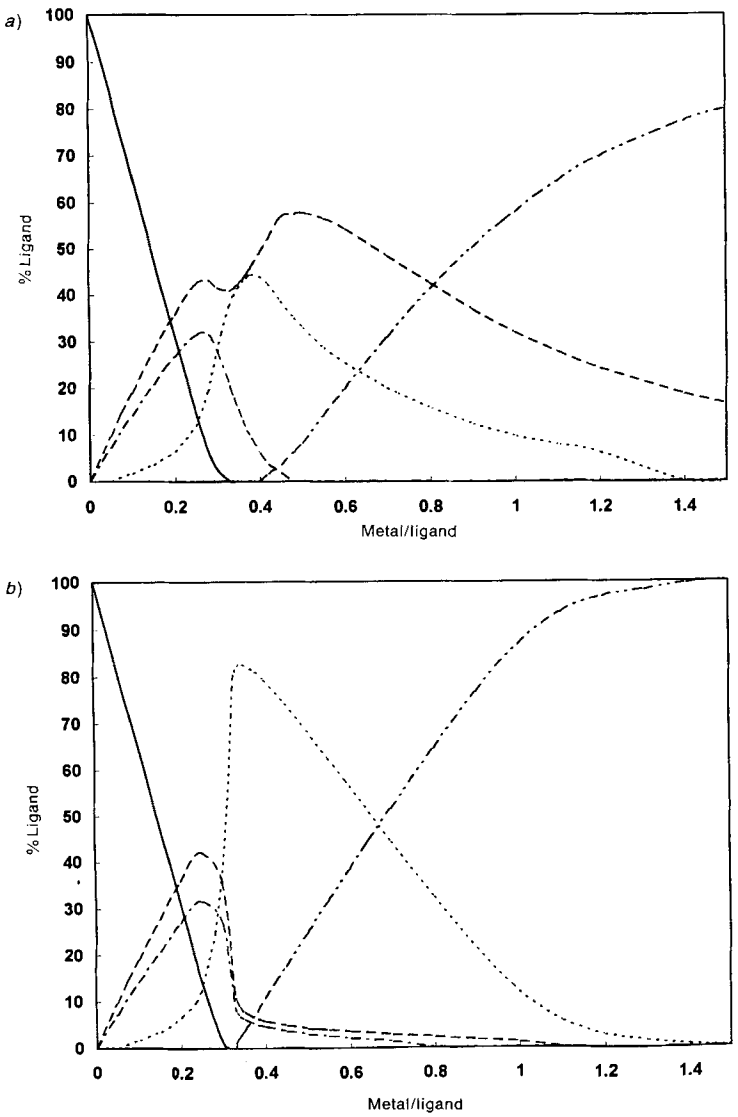

Fig. 5. *Calculated speciation of ligand for the spectrophotometric titration of* L^2 *with an equimolar mixture of* $La(ClO_4)_3 \cdot 7\ H_2O$ *and* $Zn(ClO_4)_2 \cdot 6\ H_2O$ *in MeCN for a total ligand concentration of* a) 10^{-4} M *and* b) 10^{-2} M. Metal = conc. La^{III} = conc. Zn^{II}; —— L^2, – – – – $[Zn(L^2)_2]^{2+}$; · · · · · $[LaZn(L^2)_3]^{5+}$, –·–·– $[La_2(L^2)_3]^{6+}$, and –··–··– $[Zn_2(L^2)_2]^{4+}$.

signals corresponding to $[La_2(\mathbf{L}^2)_3]^{6+}$ are detected despite its expected significant concentration, probably as a result of the excellent ES-MS response of $[LaZn(\mathbf{L}^2)_3]^{5+}$ and $[Zn(\mathbf{L}^2)_2]^{2+}$. Similar behavior is observed when La^{III} is replaced by other lanthanide ions leading to the selective formation of $[LnZn(\mathbf{L}^2)_3]^{5+}$ (Ln = Nd, Eu, Tb, Y, Lu, *Table 1*). For Eu^{III}, a value of log $(\beta_{113}^{EuZn}) = 25.3(4)$ is obtained from the spectrophotometric data (r.m.s. = 0.002). The slightly lower stability found for $[EuZn(\mathbf{L}^2)_3]^{5+}$ is probably not significant given the similarity of the UV spectra of the complexes studied.

Eqns. 1–4 predict that the concentration of $[LaZn(\mathbf{L}^2)_3]^{5+}$ should be *ca.* ten times larger than that of any other complex for Ln/Zn/$\mathbf{L}^2$ 1:1:3 and $\mathbf{L}^2_{tot} > 10^{-2}$ M (*Fig. 5b*), and this is indeed reflected in the ^{1}H-NMR spectrum where only one predominant species of high symmetry corresponding to $[LaZn(\mathbf{L}^2)_3]^{5+}$ is observed (*Fig. 6a*). Detailed NMR measurements (COSY, NOESY, NOEDIF) allow the complete assignment of the 26 signals arising from three equivalent ligands and are compatible with C_3 (or C_{3v}) symmetry on the NMR time scale. The diastereotopic protons of CH_2–C(5′) and CH_2–N(1‴) (see *Fig. 6a*) preclude the existence of mirror planes [30] and point to a C_3 head-to-head arrangement of the ligands, compatible with a triple-helical structure similar to that found for $[Ln_2(\mathbf{L}^3)_3]^{6+}$ [5]. Strong NOE's for H–C(3‴)/Me–N(1′), H–C(3″)/Me–N(1), and H–C(5″)/CH_2–N(1‴) confirm that both bidentate and tridentate binding units display s-*cis* conformations consecutive to their coordination to the metal ions (*Fig. 7a*) [13]. Further structural information is obtained from the intrastrand NOE's experienced by the protons of the spacer. Thus, irradiation of CH_a–C(5′) (or CH_b–C(5′)) gives NOE's with H–C(6′) and H–C(4) (or H–C(6) and H–C(4′), resp.), while irradiation of H–C(4) (or H–C(4′)) leads to only one additional NOE with H–C(4′) (or H–C(4), resp., *Fig. 6b*). As previously described [13], this NOE map corresponds to the conformation of the spacer depicted in *Fig. 1* (structure **V**) which results from helical torsion of the ligand. In $[FeAg(\mathbf{L}^1)_2]^{3+}$, the double-helix arrangement of the ligands $\mathbf{L}^1$ brings H–C(4) near the bisecting plane between H–C(4′) and H–C(6′), giving two strong NOE's for H–C(4)/H–C(6′) and H–C(4)/H–C(4′) [13]. For $[LaZn(\mathbf{L}^2)_3]^{5+}$, the different NOE's experienced by H–C(4) suggest a significant decrease of the dihedral angle between the benzo moieties; H–C(4) moves towards H–C(4′), the *H*–C(4)/*H*–C(4′) distance becomes shorter, and the larger *H*–C(4)/*H*–C(6′) separation is no longer expected to show a NOE in such a 'small' molecule [31]. This trend is in agreement with the large upfield shifts observed for H–C(4) (1.77 ppm) and H–C(4′) (2.48 ppm) in $[LaZn(\mathbf{L}^2)_3]^{5+}$ and which are typical of a helical twist of the ligand (1.80 ppm for $[La_2(\mathbf{L}^3)_3]^{6+}$) [5]. It is also consistent with the X-ray crystal structure of the triple-helical complex $[Eu_2(\mathbf{L}^3)_3](ClO_4)_6$ which shows that the benzo moieties of the spacer deviate from a perpendicular arrangement resulting in a *H*–C(4)/*H*–C(4′) distance (3.1–3.2 Å) significantly shorter than the *H*–C(4)/*H*–C(6′) separation (3.9–4.3 Å) [26]. In $[LaZn(\mathbf{L}^2)_3]^{5+}$, the weak interstand NOE's observed for Me–N(1)/CH_2–N(1‴) (*Fig. 6c*), Me–N(1′)/H–C(6), and Me–N(1)/H–C(6′) arise from the close packing of the strands, itself a consequence of the helical wrapping of the ligands around the C_3 axis (*Fig. 7b*), as reported for the triple-helical complexes $[Ln(\mathbf{L}^4)_3]^{3+}$ [17] [32] and $[Ln_2(\mathbf{L}^3)_3]^{6+}$ [5] [26].

The ^{1}H-NMR spectra (*Table 3*) of $[LnZn(\mathbf{L}^2)_3]^{5+}$ (Ln = Y, Lu) demonstrate the almost quantitative formation of C_3-helical complexes. They are very similar to the spectrum of the La^{III} complex, except for some minor deviations (H–C(4), H–C(4‴)) associated with the contraction of the ionic radii [33], which slightly distorts the coordination sphere

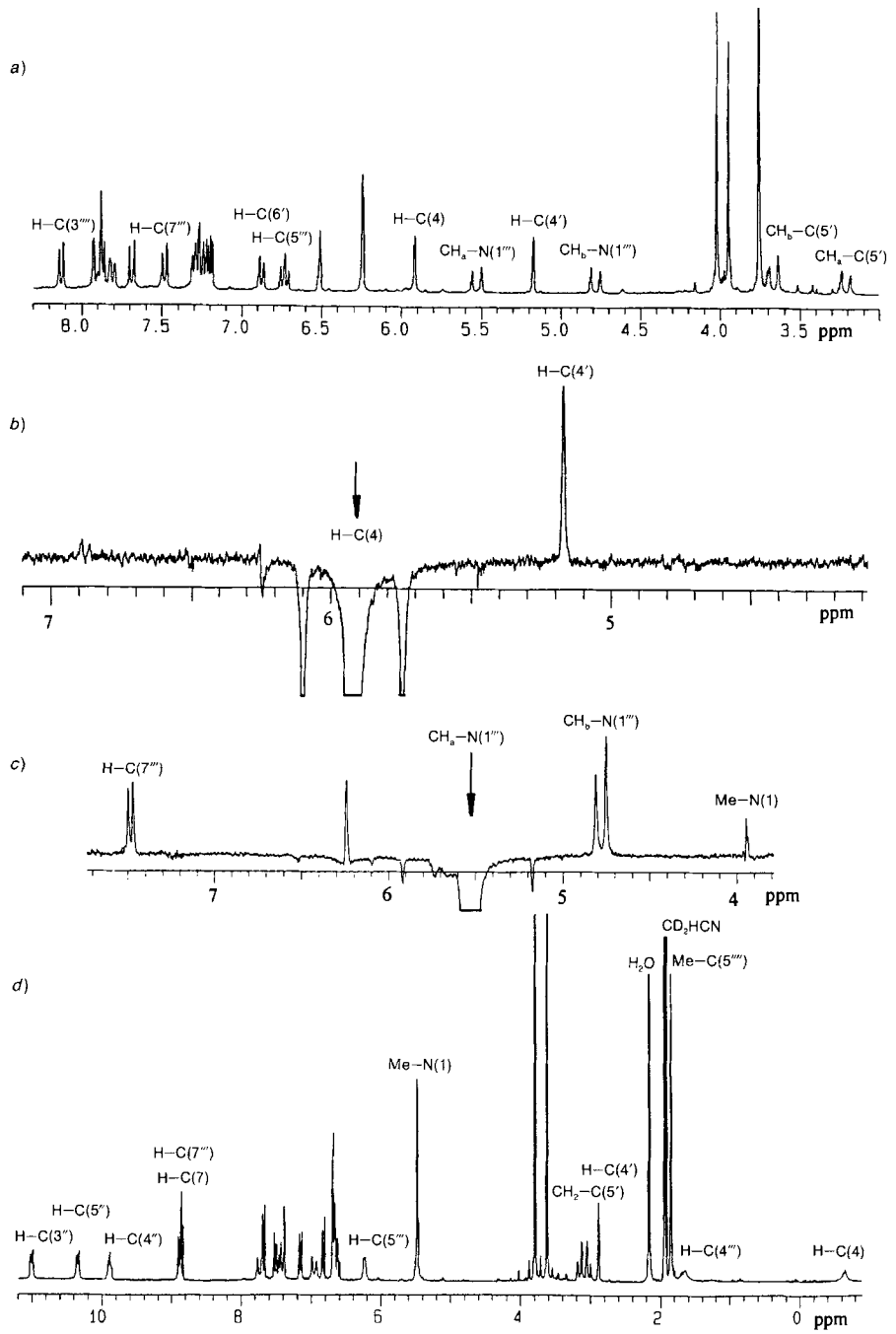

Fig. 6. a) *^{1}H-NMR Spectrum of [LaZn(L^2)$_3$]$^{5+}$*, b) *NOEDIF spectrum upon irradiation of H–C(4) of [LaZn(L^2)$_3$]$^{5+}$*, c) *NOEDIF spectrum upon irradiation of CH$_a$–N(1‴) of [LaZn(L^2)$_3$]$^{5+}$*, *and* d) *^{1}H-NMR spectrum of [NdZn(L^2)$_3$]$^{5+}$*. Total ligand concentration $2.25 \cdot 10^{-2}$ M.

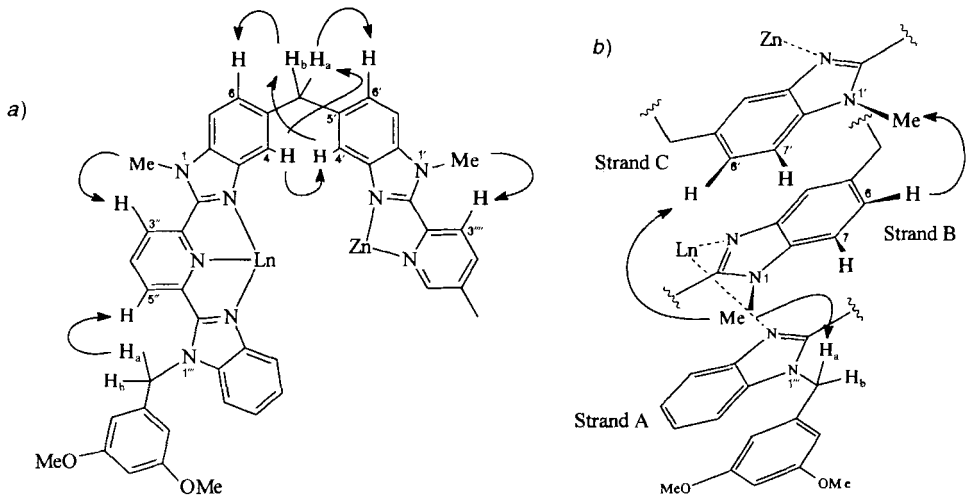

Fig. 7. *Selected* a) *intra-strand and* b) *inter-strand NOE's observed for* $[LnZn(L^2)_3]^{5+}$ (Ln = La, Ce, Pr, Nd, Sm, Eu, Y, Lu) *in* CD_3CN. Contact distances calculated from the X-ray crystal structure of $[Eu_2(L^3)_3](ClO_4)_6$ [26].

Estimated inter-strand distances [26]

CH_2–N(1‴)/*Me*–N(1)	3.5–3.8 Å
Me–N(1)/*H*–C(6′)	3.4–3.7 Å
Me–N(1′)/*H*–C(6)	3.9–4.1 Å
CH_2–N(1‴)/*H*–C(7)	4.5–4.9 Å
Me–N(1)/*H*–C(7′)	4.4–4.5 Å

around the lanthanide ion [5]. To investigate the detailed structure and the location of the two metal ions in the different coordination sites of $[LnZn(L^2)_3]^{5+}$, we used paramagnetic Ln^{III} ions as shift reagents [29]. For the axial complex $[LnZn(L^2)_3]^{5+}$, the chemical shift δ_{ij}^{exp} of the proton i in the complex with lanthanide j is given by *Eqn. 5* where δ_i^{dia} is the diamagnetic contribution to the chemical shift taken from $[LaZn(L^2)_3]^{5+}$ and $\delta_{ij}^{contact} + \delta_{ij}^{dipolar}$ is the total paramagnetic induced shift. The separation of the contact and dipolar contributions to the paramagnetic shifts of the protons according to *Eqn. 5* is rather straightforward and leads to important structural information [34] [35].

$$\delta_{ij}^{exp} = \delta_i^{dia} + \delta_{ij}^{contact} + \delta_{ij}^{dipolar} = \delta_i^{dia} + F_i \cdot \langle S_z \rangle_j + G_i \cdot C_j \qquad (5)$$

$$F_i = \frac{A_i}{g_N \beta_N} \quad \text{and} \quad G_i = \frac{a}{T^2} \left[\frac{3\cos^2(\theta) - 1}{r^3} \right]_i$$

F_i is the contact term of proton i which depends upon the delocalization of the spin density measured by the hyperfine coupling constants A_i, while G_i is the dipolar term; both are independent of the lanthanide used. At a given temperature T, G_i, is related to structural factors and to the ligand-field parameter a (θ and r are the polar coordinates relative to the principal magnetic axis for the nucleus i under investigation) [34]. The average spin values $\langle S_z \rangle_j$ [36] and *Bleaney*'s coefficients C_j [37] depend only on the lanthanide used, provided the complexes studied are isostructural [29] [34]. Therefore, a reliable separation of contact and dipolar contributions for $[LnZn(L^2)_3]^{5+}$ requires *i*) a detailed and dependable assignment of the different protons *via* 2D-COSY, 2D-NOESY, and NOEDIF experiments and *ii*) only minor changes in structural parameters along the

lanthanide series. These two conditions are fullfilled by the larger lanthanides La^{III} to Eu^{III} which possess a sufficiently short electronic relaxation time [29] to allow reliable NOE's to be detected [35]. Moreover, they do not significantly distort the cylindrical molecular architecture, as demonstrated by the similarity between the ^{1}H-NMR spectra of $[LnZn(\mathbf{L}^2)_3]^{5+}$ for Ln = La and Y (Y^{III} is smaller than Eu^{III} [33]). For $[\mathbf{L}^2_{tot}] = 2.25 \cdot 10^{-2}$ M and Ln/Zn/$\mathbf{L}^2$ 1:1:3, the formation of the helical complexes $[LnZn(\mathbf{L}^2)_3]^{5+}$ (Ln = Ce, Pr, Nd, Sm, Eu) is established by the ^{1}H-NMR spectra which show them to be the only species in solution (*Fig. 6d*). Detailed assignments of the signals are given in *Table 3*. Taking $[LaZn(\mathbf{L}^2)_3]^{5+}$ as the diamagnetic reference, the paramagnetic induced shifts $\delta_{ij}^{exp} = \delta_{ij}^{LnZn} - \delta_i^{LaZn}$ of the aromatic protons and Me groups of each $[LnZn(\mathbf{L}^2)_3]^{5+}$ complex (Ln = Ce, Pr, Nd, Sm, Eu) are fitted to *Eqn. 5* using a multiple linear regression technique [38]. Least-squared values for F_i and G_i, agreement factors (AF_i, *Eqn. 6* [34] [39]), correlation coefficients for $\langle S_z \rangle_j$ *vs.* $\delta_{ij}^{contact}$ ($\sigma^{contact}$) and C_j *vs.* $\delta_{ij}^{dipolar}$ ($\sigma^{dipolar}$) [34], and calculated corrected contact ($\delta_{corr}^{contact}$) and dipolar ($\delta_{corr}^{dipolar}$) contributions are given in *Table 4*.

$$AF_i = \sqrt{\frac{\sum_j (\delta_{ij}^{exp} - \delta_{ij}^{cal})^2}{\sum_j (\delta_{ij}^{exp})^2}} \tag{6}$$

The agreement factors and the correlation coefficients obtained for the aromatic protons are satisfying and can be compared to those found for similar mathematical treatments applied to [Ln(pyridine-2,6-dicarboxylato)$_3$]$^{3-}$ ($0.004 < AF < 0.27$ [34]) and [Ln^{III} (texaphyrin)$(NO_3)_2$] ($0.06 < AF < 0.26$ [35]). The difference between the sum of the predicted contact and dipolar contributions (*Eqn. 5*) and the experimental paramagnetic shift (δ_{ij}^{exp}) is distributed between the contact and dipolar values according to their relative contributions [34] leading to the corrected values given in *Table 4*.

Small F_i values ($F_i < 0.06$) are observed for the protons of the bidentate binding unit and for Me–N(1), H–C(6), H–C(5‴), and H–C(6‴) of the tridentate unit; therefore, spin delocalization *via* 'through bond' effects [34] is weak or negligible for these protons because of their large topological separations from the paramagnetic lanthanide ($\geq$ five bonds [40]). When the number of chemical bonds between the coordinated N-atom of the tridentate unit and the investigated proton decreases, F_i values significantly increase to reach the range 0.14–0.18 (four bonds, H–C(7),H–C(4″),H–C(7‴)) or 0.25–0.33 (three bonds, H–C(4),H–C(3″),H–C(5″),H–C(4‴)). We conclude that the paramagnetic lanthanide ion is coordinated to the tridentate binding unit *via* the central pyridine ring and the two distal benzimidazole aromatic rings. The large values of F_i calculated for the protons bound to the pyridine ring (H–C(3″),H–C(4″),H–C(5″)) contrast with those found for the same protons in [Ln(pyridine-2,6-dicarboxylato)$_3$]$^{3-}$ (0.009–0.013 [34]), which indicates a large spin delocalization when Ln^{III} is coordinated by nine heterocyclic donor N-atoms in $[LnZn(\mathbf{L}^2)_3]^{5+}$ (see photophysical properties). Assuming similar structures for $[LnZn(\mathbf{L}^2)_3]^{5+}$ (Ln = Ce, Pr, Nd, Sm, Eu), large absolute dipolar contributions G_i are limited to short distances between the protons and Ln^{III} (*Eqn. 5*). The G_i values are small for the bidentate unit, and increase significantly when the protons lie closer to the Ln^{III} ion coordinated to the tridentate unit. Maximum values are thus found for H–C(4) (0.903) and H–C(4‴) (0.737) which point toward the metal ion and provide large dipolar contributions to the paramagnetic shift. These protons give broad signals in the ^{1}H-NMR spectra, the line-width exhibiting a r^{-3} dependence, when dipolar transverse relaxation is the dominant line-broadening factor [41] (*Fig. 6d*).

Table 4. *Corrected Computed Values for Contact (δ^{cont}) and Dipolar (δ^{dip}) Contributions*

	Bidentate binding unit							
	Me–C(5‴)	Me–N(1′)	H–C(6‴)	H–C(4‴)	H–C(3‴)	H–C(7′)	H–C(6′)	H–C(4′)
F_i[b])	–0.015	–0.018	–0.029	–0.020	–0.024	–0.029	–0.022	–0.105
G_i[c])	0.037	0.055	0.067	0.038	0.061	0.051	0.030	0.030
AF_i[d])	0.13	0.13	0.12	0.10	0.11	0.09	0.08	0.14
σ^{cont}[e])	–0.995	–0.994	–0.995	–0.998	–0.996	–0.998	–0.999	–0.993
σ^{dip}[e])	0.989	0.988	0.990	0.991	0.992	0.992	0.994	0.988
δ^{cont}(CeZn)[f])	–0.01	–0.01	–0.02	–0.02	–0.02	–0.02	–0.02	–0.09
δ^{dip}(CeZn)[f])	–0.19	–0.29	–0.35	–0.19	–0.32	–0.26	–0.16	–1.60
δ^{cont}(PrZn)[f])	–0.04	–0.06	–0.09	–0.06	–0.07	–0.09	–0.07	–0.32
δ^{dip}(PrZn)[f])	–0.42	–0.62	–0.76	–0.43	–0.68	–0.58	–0.34	–3.38
δ^{cont}(NdZn)[f])	–0.08	–0.11	–0.16	–0.10	–0.13	–0.15	–0.11	–0.62
δ^{dip}(NdZn)[f])	–0.20	–0.30	–0.36	–0.19	–0.32	–0.24	–0.14	–1.68
δ^{cont}(SmZn)[f])	0.00	0.00	0.00	0.00	0.00	0.00	0.00	0.01
δ^{dip}(SmZn)[f])	–0.04	–0.04	–0.07	–0.01	–0.06	–0.04	0.00	–0.44
δ^{cont}(EuZn)[f])	0.14	0.18	0.29	0.20	0.24	0.30	0.22	1.02
δ^{dip}(EuZn)[f])	0.14	0.20	0.25	0.14	0.22	0.19	0.19	1.11

[a]) Corrected contact and dipolar contributions are given in ppm (rel. to $SiMe_4$) with $[LaZn(\mathbf{L}^2)_3]^{5+}$ as a diamagnetic reference (see text).

[b]) Contact term and

[c]) dipolar term according to *Eqn. 5*.

We conclude from the NMR data that the three ligands $\mathbf{L}^2$ are wrapped around the helical axis defined by the metal ions, leading to the C_3-helical structure **IV** for $[LnZn(\mathbf{L}^2)_3]^{5+}$ in solution. The Zn^{II} ion is coordinated by the three bidentate units in a pseudo-octahedral arrangement and the Ln^{III} ion lies in the remaining pseudo-tricapped trigonal prismatic site defined by the tridentate binding units. The assembly processes leading to the selective formation of the heterodinuclear complex $[LaZn(\mathbf{L}^2)_3]^{5+}$ are summarized in *Fig. 8*. Slow diffusion of Et_2O into concentrated MeCN solutions of heterodinuclear complexes leads to the isolation of microcrystalline powders whose elemental analyses correspond to $[LnZn(\mathbf{L}^2)_3](ClO_4)_5 \cdot n H_2O$ (Ln = La, $n = 5$, **4**; Ln = Nd, $n = 2.5$, **5**; Ln = Eu, $n = 4$, **6**; Ln = Tb, $n = 3$, **7**; Ln = Y, $n = 4$, **8**; Ln = Lu, $n = 4$, **9**). The complexes are readily soluble in MeCN and give spectra (ES-MS, ^{1}H-NMR, and UV/VIS) identical to those obtained when the complexes are prepared *in situ*. Unfortunately, we were unable to obtain crystals suitable for X-ray diffraction studies.

Photophysical Properties of Ligands $\mathbf{L}^1$ *and* $\mathbf{L}^2$ *and Complexes* $[Ln_2(\mathbf{L}^2)_3](ClO_4)_6 \cdot EtOH \cdot nH_2O$ (Ln = La, $n = 6$, **2**; Ln = Eu, $n = 11$, **3**) *and* $[LnZn(\mathbf{L}^2)_3](ClO_4)_5 \cdot nH_2O$ (Ln = La, $n = 5$, **4**; Ln = Eu, $n = 4$, **6**; Ln = Tb, $n = 3$, **7**; Ln = Y, $n = 4$, **8**; Ln = Lu, $n = 4$, **9**). Reflectance spectra of the free ligands $\mathbf{L}^1$ and $\mathbf{L}^2$ are almost identical and display one main band at 29600 cm^{-1} with a shoulder at 28600 cm^{-1}. We assign these features to $\pi \rightarrow \pi^*$ transitions, since $n \rightarrow \pi^*$ transitions have a much weaker intensity [16]. The $^1\pi\pi^*$ state of $\mathbf{L}^1$ and $\mathbf{L}^2$ are close in energy to the levels observed for $\mathbf{L}^3$ (28100 and 30100 cm^{-1}) [5] and for $\mathbf{L}^4$ (27800 cm^{-1}) [42]. Luminescence is observed at 77 K upon excitation to these singlet states (*Fig. 9*): one band appears at 24200 ($\mathbf{L}^1$) or 25000 ($\mathbf{L}^2$) cm^{-1}, while a weak triplet-state emission is seen at 19200 cm^{-1}. Both bands are structured. The $^3\pi\pi^*$ luminescence decay is multi-exponential and temperature-depen-

to the Paramagnetic Experimental ^{1}H-NMR Shifts for $[LnZn(L^2)_3]^{5+}$[a])

Tridentate binding unit										
Me–N(1)	H–C(4)	H–C(6)	H–C(7)	H–C(3″)	H–C(4″)	H–C(5″)	H–C(7‴)	H–C(6‴)	H–C(5‴)	H–C(4‴)
0.060	–0.248	–0.03	0.143	0.335	0.178	0.337	0.144	–0.003	–0.039	–0.255
–0.202	0.903	0.017	–0.078	–0.250	–0.207	–0.242	–0.118	–0.030	0.057	0.737
0.17	0.15	0.27	0.09	0.11	0.09	0.10	0.10	0.14	0.11	0.14
0.990	–0.992	–0.967	0.998	0.997	0.997	0.997	0.997	–0.986	–0.996	–0.993
–0.983	0.987	0.962	–0.994	–0.990	–0.995	–0.991	–0.993	–0.987	0.989	0.987
0.05	–0.20	0.00	0.12	0.26	0.16	0.27	0.12	0.00	–0.03	–0.21
1.02	–4.77	–0.10	0.42	1.27	1.16	1.22	0.64	0.17	–0.29	–3.81
0.18	–0.74	–0.01	0.43	1.02	0.53	1.02	0.43	–0.01	–0.12	–0.77
2.25	–10.03	–0.17	0.86	2.80	2.28	2.72	1.30	0.36	–0.65	–8.23
0.37	–1.49	–0.02	0.77	1.83	0.96	1.82	0.79	–0.02	–0.22	–1.50
1.17	–5.08	–0.12	0.39	2.28	1.05	1.22	0.61	0.19	–0.29	–4.05
–0.01	0.03	0.00	–0.01	–0.03	–0.01	–0.03	–0.01	0.00	0.00	0.04
0.33	–1.42	–0.05	0.05	0.27	0.10	0.24	0.11	0.03	–0.06	–1.23
–0.57	2.38	0.03	–1.46	–3.41	–1.80	–3.44	–1.46	0.02	0.39	2.48
–0.72	3.25	0.05	–0.30	–0.95	–0.79	–0.92	–0.45	–0.10	0.22	2.68

[d]) Agreement factor as defined in *Eqn. 6*.

[e]) Correlation coefficients for contact and dipolar contributions [34] (see text).

[f]) δ^{cont}(LnZn) is the corrected contact contribution in ppm for the complex $[LnZn(L^2)_3]^{5+}$ and δ^{dip}(LnZn) the corresponding dipolar contribution.

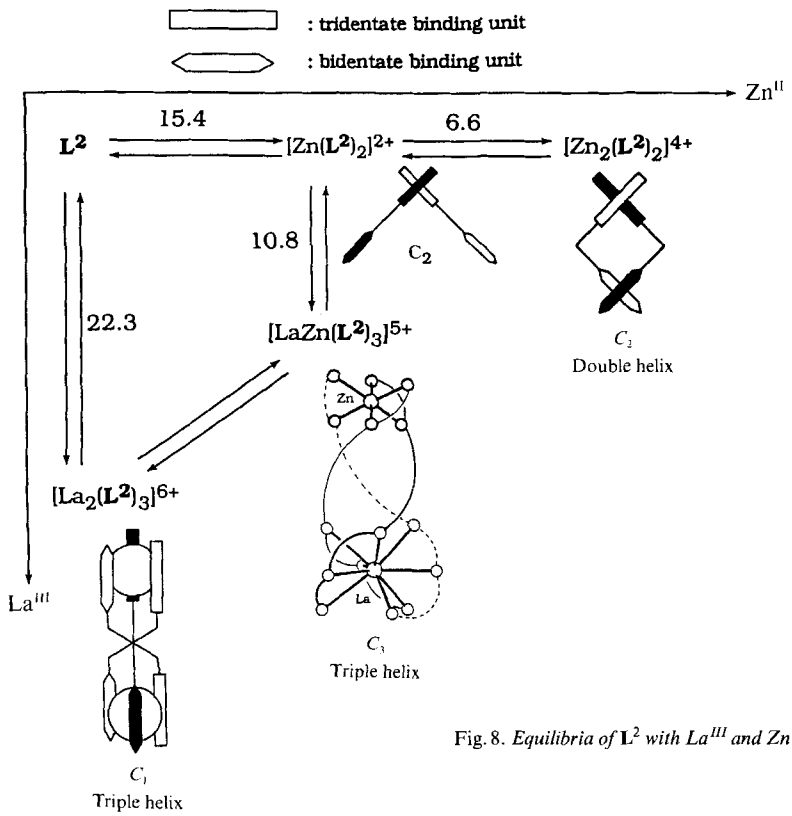

Fig. 8. *Equilibria of* L^2 *with* La^{III} *and* Zn^{II} *in MeCN*

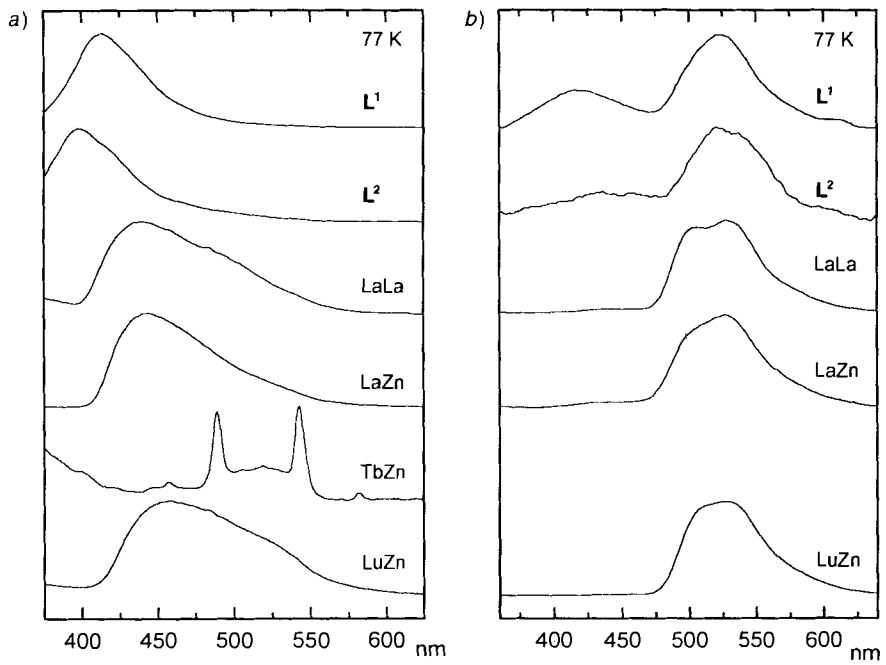

Fig. 9. *Emission bands of the ligands at 77 K for powdered samples of* L^1, L^2, $[La_2(L^2)_3](ClO_4)_6 \cdot n$ *solv.* (**2**; LaLa), *and* $[LnZn(L^2)_3](ClO_4)_5 \cdot n$*solv.* (*LnZn*), *upon excitation at 340 nm:* a) *continuous spectra*, b) *time-resolved spectra* (delay 0.25 s). Vertical scale: arbitrary units.

Table 5. *Lifetimes* τ [ms] *of the Ligand Triplet States, as Determined from Multi-Parameter Least-Squares Analysis.* λ_{exc} 308 nm, λ_{an} 540 nm, standard deviations are given in parentheses.

	τ(77 K)/ms		τ(10 K)/ms	
L^3 [a])	372(31)	82(8)	660(10)	132(6)
L^4	190(10)		323(14)[b])	
L^1	161(16)	20(2)	769(9)	228(16)
L^2	347(52)	87(8)	719(30)	244(43)
$[La_2(L^2)_3](ClO_4)_6 \cdot EtOH \cdot 6\ H_2O$ (**2**)	69(2)		201(2)	63(2)
$[LaZn(L^2)_3](ClO_4)_5 \cdot 5\ H_2O$ (**4**)	124(2)	37(6)	225(32)	84(20)
$[YZn(L^2)_3](ClO_4)_5 \cdot 4\ H_2O$ (**8**)	408(17)	82(9)	473(12)	93(9)
$[LuZn(L^2)_3](ClO_4)_5 \cdot 4\ H_2O$ (**9**)	243(69)	79(10)	319(52)	82(8)

[a]) A value of $\tau = 4.4$ ms was wrongly reported in [5]. [b]) At 4.2 K, from [42].

dent. Two different lifetimes are extracted from the 10 K data using a multi-parameter mathematical analysis (*Table 5*). They arise from the two different coordinating regions of the ligand.

Upon complexation, the splitting of the two observed $\pi \rightarrow \pi^*$ transitions increases from *ca.* 1000 cm^{-1} for L^2 to 3400 cm^{-1} for the La complexes and 4500 cm^{-1} for the Eu- and Y-containing complexes (*Table 6*). The splitting of the $^3\pi\pi^*$ state follows the same trend, increasing from 550 cm^{-1} for L^2 to 800–1000 cm^{-1} for the La complexes. The lifetimes of

Table 6. *Observed $\pi \rightarrow \pi^*$ Transitions and Energies of the Singlet and Triplet States* [cm^{-1}] *in the Complexes with* L^2, *as Determined from Reflectance and Emission Spectra at 77 K*

	$\pi \rightarrow \pi^*$	$\pi \rightarrow \pi^*$	$^1\pi\,\pi^*$	$^3\pi\,\pi^*$	$^3\pi\,\pi^*$
L^2	29600	28600(sh)	25000	19200	18650
$[La_2(L^2)_3](ClO_4)_6 \cdot EtOH \cdot 6\,H_2O$ (**2**)	29600	26200	22800	20000(sh)	19000
$[Eu_2(L^2)_3](ClO_4)_6 \cdot EtOH \cdot 11\,H_2O$ (**3**)	29850	25500	[a])	[b])	[b])
$[LaZn(L^2)_3](ClO_4)_5 \cdot 5\,H_2O$ (**4**)	29600	26200	22600	19700	18900
$[EuZn(L^2)_3](ClO_4)_5 \cdot 4\,H_2O$ (**6**)	29950	25500	[a])	[b])	[b])
$[TbZn(L^2)_3](ClO_4)_5 \cdot 3\,H_2O$ (**7**)	29950	25600	[a])	[c])	[c])
$[YZn(L^2)_3](ClO_4)_5 \cdot 4\,H_2O$ (**8**)	30300	25650	21800	19200[c])	[c])
$[LuZn(L^2)_3](ClO_4)_5 \cdot 4\,H_2O$ (**9**)	30300	25650	22200	19700	18900

[a]) Not observed. [b]) Masked by Eu luminescence. [c]) Masked by Tb luminescence (*cf.* text).

the triplet states in the complexes are shorter than in the free ligand, as was observed for complexes with ligands analogous to L^4 [17]. A substantial antenna effect is observed for both the Eu- and Tb-containing complexes. When excited through the $\pi \rightarrow \pi^*$ transitions, the emission spectra of microcrystalline samples display essentially the sharp bands arising from the $Eu(^5D_0)$ and $Tb(^5D_4)$ excited levels, in addition to a weak triplet emission. Also, the luminescence spectrum of the heterodinuclear complex $[YZn(L^2)_3](ClO_4)_5$ (**8**) contains sharp bands attributable to Tb^{III} impurities (less than 0.01%).

The Eu- and Tb-containing compounds are very weakly luminescent at room temperature, and no emission band can be measured in 10^{-2} M solutions. We, therefore, examined the excitation and emission spectra of these compounds at 77 and 10 K in the solid state. The Eu complexes were investigated in greater detail, to determine the influence of replacing one Eu^{III} ion by Zn^{II} when going from structures **III** to **IV** (*Fig. 1*). The excitation spectrum at 10 K in the region of the $^5D_0 \leftarrow {}^7F_0$ transition reveals the presence of a single broad band centered at 17224 cm^{-1} for the heterodinuclear complex $[EuZn(L^2)_3](ClO_4)_5 \cdot 4H_2O$ (**6**) and at 17231 cm^{-1} for the homodinuclear complex $[Eu_2(L^2)_3](ClO_4)_6 \cdot EtOH \cdot 11\,H_2O$ (**3**). It is symmetrical for **6** (full width at half height (f.w.h.h.) = 25 cm^{-1}) and slightly asymmetrical on the high-energy side for **3** (f.w.h.h. = 26 cm^{-1}). The corresponding emission bands ($^5D_0 \rightarrow {}^7F_0$) obtained upon excitation through the ligand states are perfectly symmetrical and slightly narrower. They appear at 17214 cm^{-1} (f.w.h.h. = 24 cm^{-1}) for **6** and at 17225 cm^{-1} (f.w.h.h. = 22 cm^{-1}) for **3**. The band width of the 0–0 transition is indicative of how well defined the Eu chemical environment is. A width greater than 10 cm^{-1} occurs when the investigated compound contains a statistical distribution of molecules having somewhat different conformations [43] [44]. The broad 0–0 transitions observed for both **6** and **3** do not allow us to detect the presence of different chemical environments arising from the two nucleating parts of the ligand. They point to the complexes being either amorphous (single crystals could not be grown) or having a rather large fluxionality which could arise from the presence of the dimethoxybenzyl groups [13].

The low energy $\tilde{\nu}$ of the $^5D_0 \leftarrow {}^7F_0$ transition is typical of Eu^{III} coordinated to nine heterocyclic N-atoms [5] [17] [32] and suggests a particularly large nephelauxetic parameter for this type of donor atoms. *Frey* and *Horrocks* recently proposed a correlation between the energy of the $^5D_0 \leftarrow {}^7F_0$ transition and parameters describing the ability δ of

coordinating atoms to produce a nephelauxetic effect [38]: $\tilde{\nu} - \tilde{\nu}_0 = C_{CN}\Sigma n_i\delta_i$ where C_{CN} is a coefficient depending upon the Eu^{III} coordination number CN (1.0 for CN = 9), n_i the number of atoms of type i, and $\tilde{\nu}_0 = 17374\ cm^{-1}$ at 295 K. For a 9-coordinate species, the value given for an amine N-atom (AN) is $\delta_{AN} = -12.1$ [38], henceforth a predicted value of 17253 cm^{-1} at 10 K (the temperature dependence is 1 cm^{-1} per 24 K [43]). The large discordance with the data reported in this work means that heterocyclic N-atoms tend to produce a larger nephelauxetic effect than aliphatic ones, contrary to what is assumed in [38]. Taking into account the energies found for 6 $^5D_0 \leftarrow {}^7F_0$ transitions reported for Eu environments containing 9 heterocyclic N-atoms [5] [17] [32], we find an average value, corrected to 295 K, $\tilde{\nu} = 17237\ cm^{-1}$ (range: 17228–17245 cm^{-1}), leading to $\delta_{HN} = -15.3$. It is noteworthy that the $\tilde{\nu}$ value reported for the heterodinuclear complex **6** fits exactly these data: 17236 cm^{-1} (295 K). In the homodinuclear complex **3**, the two metal sites contain 8 and 7 heterocyclic N-atoms. Assuming the latter are the only coordinated ligands, we find a mean value $\tilde{\nu} = 17244\ cm^{-1}$ (experimental value: 17243 at 295 K). Supposing the coordination sphere is completed to CN = 9 by perchlorate O-atoms induces too low $\tilde{\nu}$ values, while a completion of the environment by H_2O molecules would correspond to values in the range 17241 to 17246 cm^{-1}. Lifetime measurements, however (*vide infra*), proscribes this assumption. The nephelauxetic effect evidenced here is in qualitatively good agreement with the large spin delocalization observed by ^{1}H-NMR for these complexes.

The luminescence spectra obtained upon excitation through the ligand bands or through the 0–0 transition are similar for the two complexes (*Fig. 10*). The relative, corrected and integrated intensities of the $^5D_0 \leftarrow {}^7F_J$ transitions for **6** (EuZn) at 10 K are 0.01, 1.0, 2.1, 0.2, and 2.1 ($J = 0$, 1, 2, 3, and 4, resp.); these intensities do not vary

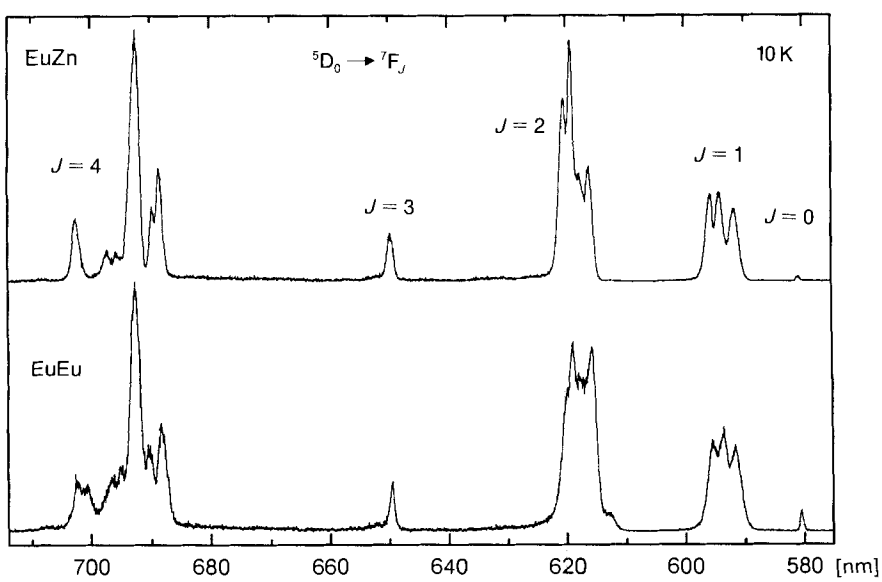

Fig. 10. *Emission spectra of* $[EuZn(L^2)_3](ClO_4)_5 \cdot 4\ H_2O$ (**6**; EuZn) *and* $[Eu_2(L^2)_3](ClO_4)_6 \cdot EtOH \cdot 11\ H_2O$ (**3**; EuEu) *samples at 10 K.* $\lambda_{ex} = 400$ nm. Vertical scale: arbitrary units.

Table 7. *Eu(^7F_J) Identified Levels* (cm^{-1}, J = 1–4) *in* $[Eu_2(L^2)_3](ClO_4)_6 \cdot EtOH \cdot 11\ H_2O$ (**3**) *and* $[EuZn(L^2)_3](ClO_4)_5 \cdot 4\ H_2O$ (**6**), *as Calculated from Luminescence Spectra at 77 and 10 K.* λ_{exc} 400 nm

Level	6		3	Level	6		3
	77 K	10 K	10 K		77 K	10 K	10 K
$^7F_1$	317	315	315	$^7F_3$	1829	1825	1835
	386	387	384				
	432	430	434	$^7F_4$	2694	2694	2700
					2717	2717	2745
$^7F_2$	987	987	991		2780	2774	2792
	1031	1027	1043		2838	2843	2844
	1074	1067	1074		2878	2874	2874
	1097	1097	1098		2985	2981	2958
							2992

substantially when the temperature is increased to 77 K. For **3** (EuEu) at 10 K, the corresponding values are 0.03, 1.0, 2.1, 0.1, and 2.2 (J = 0, 1, 2, 3, and 4, resp.). The crystal-field levels identified from the luminescence spectra are listed in *Table 7*. The $^7F_1$ levels are split into three components, separated at 10 K by 72 and 43 cm^{-1} (**6**) and 69 and 50 cm^{-1} (**3**). This is typical of a large distortion from the trigonal symmetry: in $[Eu_2(L^3)_3](ClO_4)_6$, the Eu-sites of which were shown by X-ray crystallography to have a local symmetry close to D_3, these splittings amount to 118 and 18 cm^{-1}, respectively [5]. The splitting of the higher-energy components being smaller for the heterodinuclear complex **6**, we conclude that the Eu-site is slightly more symmetrical than the metal-ion sites in the homodinuclear complex. In the latter, one expects to untangle two sites with different symmetry, one Eu^{III} ion being coordinated by 8 N-donors while the other is bound to 7 N-atoms only. The amorphous nature of the compound, however, prevents such a discrimination, the emission bands remaining broad even at very low temperature. The luminescence spectra thus reflect an average coordination environment which appears to be less symmetrical. The rather strong intensities of the $^5D_0 \rightarrow {}^7F_2$ and $^5D_0 \rightarrow {}^7F_4$ transitions and the analysis of the $^7F_2$ and $^7F_4$ splittings confirm that the Eu^{III} ions lie in sites with low symmetry in both the homo- and heterodinuclear complexes. Taking into account the low oscillator strength of the 0–0 transitions, the emission spectra reflect a pseudo-D_2 site symmetry. The Eu($^5D_0$) lifetimes (*Table 8*) remain approximately constant

Table 8. *Lifetimes* τ [ms] *of the Eu($^5D_0$) and Tb($^5D_4$) Levels in Homo- and Heterodinuclear Complexes with* L^2 *Measured at 77 K and 10 K under Various Excitation Conditions,* λ_{an} was set on the maximum of the $Eu(^5D_0 \rightarrow {}^7F_2)$ or $Tb(^5D_4 \rightarrow {}^7F_5)$ transition. Standard deviations are given in parentheses.

	λ_{exc}/nm	T/K	τ/ms
$[Eu_2(L^2)_3](ClO_4)_6 \cdot EtOH \cdot 11\ H_2O$ (**3**)	308	77	2.05(5)
	308	10	2.22(7)
$[EuZn(L^2)_3](ClO_4)_5 \cdot 4\ H_2O$ (**6**)	308	77	1.97(15)
	308	10	2.30(5)
	400	77	2.12(6)
	400	10	1.96(7)
	580.6	10	2.03(8)
$[TbZn(L^2)_3](ClO_4)_5 \cdot 3\ H_2O$ (**7**)	308	10	1.17(4)
	488	10	1.36(6)

between 10 and 77 K. They are almost independent of the excitation mode and of the nature of the cation bound in the bidentate unit of the ligand. Their values are comparable to those obtained with other triple-helical complexes with $\mathbf{L}^3$ [5] or with substituted benzimidazole-pyridine ligands and reflect a good protection of the lanthanide ion from external interactions. In particular, these data point to the absence of H_2O molecules in the inner-coordination sphere of the Eu^{III} ion.

The luminescence of the heterodinuclear complex **7** (TbZn) is very weak. Upon excitation through the ligand band, one observes transitions from the $Tb(^5D_4)$ level to the ^7F_J manifold. At 10 K, the relative, integrated and corrected intensities are 1.0, 3.2, 1.0, 0.65, 0.15, and 0.05 ($J = 6$, 5, 4, 3, 2, and 1, resp.; the transition to $^7F_0$ is extremely faint). Since the ligand luminescence is weakened by the introduction of Tb^{III} in the complexes, the quenching of the Tb^{III} emission is due to a back transfer of energy from the lanthanide ion to the ligand, as already observed for many other similar compounds [5] [17]. This leads to a $Tb(^5D_4)$ lifetime considerably smaller than the one measured for $Eu(^5D_0)$, in spite of the larger energy gap $^5D_4$–$^7F_6$ as compared to $^5D_0$–$^7F_0$.

Conclusion. – The segmental ligand $\mathbf{L}^2$ possesses two binding units which, at first sight, appear rather similar since they differ only in their denticity, the ligating atoms (heterocyclic N-atoms) and the chelate angle remaining constant. Therefore, we would not expect a great selectivity upon complexation [13], which is confirmed by the coordination of both binding units in the homodinuclear complexes $[Zn_2(\mathbf{L}^2)_2]^{4+}$ and $[La_2(\mathbf{L}^2)_3]^{6+}$. However, spectroscopic studies show that an equimolar mixture of Zn^{II} and Ln^{III} (Ln = La, Ce, Pr, Nd, Sm, Eu, Tb, Y, Lu) reacts with three equivalents of $\mathbf{L}^2$ to give selectively the heterodinuclear complexes $[LnZn(\mathbf{L}^2)_3]^{5+}$ in MeCN solution where the three strands are wrapped around the C_3 axis defined by the two metal ions, producing a close-packed cylindrical structure. Detailed ^{1}H-NMR studies show that Zn^{II} is pseudo-octahedrally coordinated by the three bidentate units while Ln^{III} occupies the pseudo-tricapped prismatic site produced by the remaining tridentate units. *Eqns. 1–4* allow the calculation of the equilibrium of *Eqn. 7* which, in spite of the large uncertainties, demonstrates the stability of the heterodinuclear species.

$$4[LnZn(\mathbf{L}^2)_3]^{5+} \rightleftarrows 2[Ln_2(\mathbf{L}^2)_3]^{6+} + [Zn_2(\mathbf{L}^2)_2]^{4+} + 2[Zn(\mathbf{L}^2)_2]^{2+} \quad \log(K^{La}) = -7(4) \quad (7)$$

$$\log(K^{Eu}) = -2(4)$$

This illustrates one of the virtues of thermodynamic self-assembly which selectively produces the species maximizing the entropic and enthalpic factors under controlled external conditions (concentration, solvent, temperature) [1] [13] [45]. In the case of $\mathbf{L}^2$, Zn^{II} has a marked preference for coordination to the tridentate unit as exemplified by the quantitative formation of $[Zn(\mathbf{L}^2)_2]^{2+}$. This is unfavorable for the assembly of the heterodinuclear complex, but the low affinity of Ln^{III} for bidentate heterocyclic units [25] more than compensates this negative factor and leads to the observed selectivity in the self-assembly process.

In the heterodinuclear complexes $[LnZn(\mathbf{L}^2)_3]^{5+}$, we may consider that Zn^{II} occupies the capping position of the molecular structure, thus organizing the strands for the coordination of Ln^{III}. This thermodynamic control of the final structure prevents the facial-meridional isomerization and leads to pure facial pseudo-tricapped trigonal prismatic building blocks around Ln^{III} ideally suited for the detailed investigation of their

electronic and photophysical properties. For $[LnZn(\mathbf{L}^2)_3]^{5+}$ (Ln = Eu, Tb), the low luminescence observed, although expected [17], strongly limits the use of these building blocks for the assembly of luminescent probes [43]. However, substitution of the terminal benzimidazole groups by carboxylic-acid derivatives should increase the quantum yields and the selectivity, and permit the isolation of stable heterodinuclear d–f complexes with controlled structural, photophysical, and magnetic properties.

The photophysical data demonstrate that the compounds have an amorphous structure in the solid state, preventing a detailed exploration of their molecular structure. The similarity of the spectral and lifetime data for the complexes **3** (EuEu) and **6** (EuZn), however, shows that the replacement of the Zn^{II} ion by a trivalent lanthanide ion has little effect on the overall organization of the dinuclear complexes. Moreover, the discussion on the nephelauxetic effect tends to prove that the solid-state structure is close to the solution structure unravelled by NMR data. The weak f–f luminescence at room temperature is not due to poor energy transfer between the ligand and the metal ion but, probably, to the relatively large flexibility of the ligand, the vibrations of which provide efficient deactivation paths for the excited $Eu(^5D_0)$ state.

We gratefully acknowledge Ms. *Véronique Foiret* and Mr. *Bernard Bocquet* for their technical assistance, *J.-C.B.* thanks the *Fondation Herbette*, Lausanne, for the gift of spectroscopic equipment. This work is supported through grants from the *Swiss National Science Foundation*.

Experimental Part

General. Solvents and starting materials were purchased from *Fluka AG*, Buchs, Switzerland, and used without further purification, unless otherwise stated. The ligand *2-{6-[1-(3,5-dimethoxybenzyl)-1*H*-benzimidazol-2-yl]pyridin-2-yl}-1,1'-dimethyl-5,5'-methylene-2'-(5-methylpyridin-2-yl)bis[1*H*-benzimidazole]* ($\mathbf{L}^2$) was prepared according to a published procedure [11]. The perchlorate salts $Ln(ClO_4)_3 \cdot n H_2O$ (Ln = La, Pr, Nd, Sm, Eu, Tb, Y, Lu; $n \approx 6$–8) were prepared from the corresponding oxide (*Glucydur*, 99.99%) according to a literature method [46]. $Ce(ClO_4)_3 \cdot 5.8\ H_2O$ was obtained by metathesis of cerium(III) carbonate hydrate (*Aldrich*, 99.9%) with aq. perchloric acid.

*Bis{2-{6-[1-(3,5-dimethoxybenzyl)-1*H*-benzimidazol-2-yl]pyridin-2-yl}-1,1'-dimethyl-5,5'-methylene-2'-(5-methylpyridin-2-yl)bis[1*H*-benzimidazole]}dizinc(II) Tetraperchlorate–Water (1/4)* ($[Zn_2(\mathbf{L}^2)_2](ClO_4)_4 \cdot 4\ H_2O$; **1**). A 10^{-2} M MeCN soln. of $Zn(ClO_4)_2 \cdot 6\ H_2O$ ($7.04 \cdot 10^{-2}$ mmol, 7.03 ml) was slowly added to 50 mg ($7.04 \cdot 10^{-2}$ mmol) of $\mathbf{L}^2$ in 10 ml of CH_2Cl_2/MeCN 1:1. The resulting soln. was evaporated, the solid residue dissolved in MeCN, and MeOH slowly diffused into the soln. for 4 days: 57.7 mg (78%) of **1**. Pale yellow microcrystals.

*Tris{2-{6-[1-(3,5-dimethoxybenzyl)-1*H*-benzimidazol-2-yl]pyridin-2-yl}-1,1'-dimethyl-5,5'-methylene-2'-(5-methylpyridin-2-yl)bis[1*H*-benzimidazole]}dilanthanide(III) Hexaperchlorate–Ethanol–Water (1/1/n)* ($[Ln_2(\mathbf{L}^2)_3](ClO_4)_6 \cdot C_2H_5OH \cdot n H_2O$; Ln = La, $n = 6$, **2**; Ln = Eu, $n = 11$, **3**). A 10^{-2} M MeCN soln. of $Ln(ClO_4)_3 \cdot n H_2O$ (Ln = La, Eu $4.69 \cdot 10^{-2}$ mmol, 4.69 ml) was slowly added to 50 mg ($7.04 \cdot 10^{-2}$ mmol) of $\mathbf{L}^2$ in 10 ml of CH_2Cl_2/MeCN 1:1. The resulting soln. was evaporated and the solid residue suspended and stirred vigorously in EtOH (30 ml) for 30 min. After being cooled at −20° for 2 h, the pale yellow (Ln = La) or yellow (Ln = Eu) powder was filtered, washed with Et_2O, and dried under vacuum: 52.6 mg (79%) of **2** or 64.3 mg (93%) of **3**.

*Tris{2-{6-[1-(3,5-dimethoxybenzyl)-1*H*-benzimidazol-2-yl]pyridin-2-yl}-1,1'-dimethyl-5,5'-methylene-2'-(5-methylpyridin-2-yl)bis[1*H*-benzimidazole]}lanthanide(III)zinc(II) Pentaperchlorate–Water (1/n)* ($[LnZn(\mathbf{L}^2)_3](ClO_4)_5 \cdot n H_2O$; Ln = La, $n = 5$, **4**; Ln = Nd, $n = 2.5$, **5**; Ln = Eu, $n = 4$, **6**; Ln = Tb, $n = 3$, **7**; Ln = Y, $n = 4$, **8**; Ln = Lu, $n = 4$, **9**). A soln. of $2.34 \cdot 10^{-2}$ mmol of $Ln(ClO_4)_3 \cdot n H_2O$ (Ln = La, Nd, Eu, Tb, Y, Lu; $n = 6$–8) and 8.7 mg ($2.34 \cdot 10^{-2}$ mmol) of $Zn(ClO_4)_2 \cdot 6H_2O$ in MeCN (5 ml) was slowly added to 50 mg ($7.04 \cdot 10^{-2}$ mmol) of $\mathbf{L}^2$ in 10 ml of CH_2Cl_2/MeCN 1:1. After stirring at r.t. for 1 h, the soln. was evaporated, the solid residue dissolved in MeCN, and Et_2O slowly diffused into the soln. for 2–3 days. The resulting precipitate was collected by filtration and dried: 78–89% of **4** (Ln = La, $n = 5$), **5** (Ln = Nd, $n = 2.5$), **6** (Ln = Eu, $n = 4$), **7** (Ln = Tb, $n = 3$), **8** (Ln = Y, $n = 4$), or **9** (Ln = Lu, $n = 4$).

Complexes **1**–**9** were characterized by their IR spectra. Elemental analyses (C,H,N) were performed by Dr. *H. Eder* of the Microchemical Laboratory of the University of Geneva. Metal content was determined using internal standards by atomic absorption (*Pye Unicam SP9*) for zinc and by ICP (*PE Plasma 1000*) for lanthanides after acidic mineralization of the complexes (*Table 9*).

Table 9. *Elemental Analyses for Complexes* **1**–**9** (in %). Calculated values are given in parentheses.

	Ln	Zn	C	H	N
1	–	6.3(6.2)	52.3(52.2)	4.3(4.4)	11.8(11.4)
2	8.5(8.8)	–	50.9(50.9)	4.4(4.2)	10.6(10.6)
3	9.3(9.3)	–	48.5(49.1)	4.3(4.4)	10.2(10.3)
4	4.7(4.8)	2.3(2.2)	54.5(54.2)	4.5(4.3)	11.4(11.5)
5	5.1(5.0)	2.3(2.3)	55.2(55.0)	4.3(4.2)	11.6(11.8)
6	5.2(5.2)	2.3(2.2)	54.6(54.3)	4.4(4.2)	11.5(11.5)
7	5.8(5.5)	2.3(2.3)	54.9(54.5)	4.4(4.2)	11.5(11.6)
8	3.2(3.1)	2.3(2.3)	55.8(55.5)	4.4(4.3)	11.8(11.8)
9	6.5(6.0)	2.3(2.2)	53.8(53.9)	4.2(4.2)	11.6(11.4)

$[LnZn(L^2)_3](ClO_4)_5$ (Ln = Ce, **10**; Ln = Pr, **11**; Ln = Sm, **12**). These complexes were prepared *in situ* for ^{1}H-NMR studies in soln. A 10^{-2} M MeCN soln. of $Ln(ClO_4)_3 \cdot nH_2O$ (Ln = Ce, Pr, Sm) and $Zn(ClO_4)_2 \cdot 6\ H_2O$ (263 µl, $5.26 \cdot 10^{-3}$ mmol) was added to 11.2 mg ($1.58 \cdot 10^{-2}$ mmol) of L^2 in 5 ml of CH_2Cl_2/MeCN 1:1. After evaporation, the solid residue was dried under vacuum and then dissolved in 700 µl of CD_3CN to give $7.5 \cdot 10^{-3}$ M $[LnZn(L^2)_3](ClO_4)_5$ (Ln = Ce, **10**; Ln = Pr, **11**; Ln = Sm, **12**) which was used without further purification.

Caution! Perchlorate salts combined with organic ligands are potentially explosive and should be handled with the necessary precautions [47].

Physical Measurements. Reflectance spectra: as finely grounded powders dispersed in MgO (5%) with MgO as reference. UV/VIS Spectra: at 20° from 10^{-3} M MeCN solns.; *Perkin-Elmer-Lambda-5* and *-Lambda-7* spectrometers using quartz cells of 0.1- and 0.01-cm path length. Spectrophotometric titrations were performed with a *Perkin-Elmer-Lambda-5* spectrophotometer connected to an external computer. In a typical experiment, 50 ml of ligand (L^2) in MeCN (10^{-4} M) were titrated with a 8.3–10^{-4} M MeCN soln. of $Ln(ClO_4) \cdot nH_2O$ and $Zn(ClO_4)_2 \cdot 6\ H_2O$ at 20°. After each addition of 0.20 ml, the absorbances at 10 different wavelengths were recorded using a 0.1-cm quartz cell and transferred to the computer. Plots of extinction as a function of the metal/ligand ratio gave a first indication of the number and stoichiometry of the complexes formed; factor analysis [22] was then applied to the data to confirm the number of different absorbing species. Finally, a model for the distribution of species was fitted with a nonlinear least-squares algorithm to give stability constants as previously described [9]. IR Spectra: KBr pellets; *Perkin-Elmer-883* spectrometer. ^{1}H-NMR Spectra: at 21°; *Varian-Gemini-300* spectrometer; chemical shifts δ in ppm rel. to $SiMe_4$. ES Mass spectra: pneumatically-assisted electrospray (ES; ion spray); 10^{-4} M MeCN solns.; *API–III* tandem mass spectrometer (*PE Sciex*) by infusion at 4–10 µl/min; recording under low up-front declustering or collision induced dissociation (CID) conditions, typically ΔV = 0–30 V between the orifice and the first quadrupole of the spectrometer [18]; total charge (z) determination of the complexes by using the isotopic pattern ($z \leq 3$) or adduct ions with perchlorate anions ($z > 3$) [19]. High-resolution, laser-excited luminescence measurements: for experimental procedures, see [42] [44]; solid-state samples were finely powdered and low-temperature (77 or 10 K) was achieved by means of a *Cryodyne* (model *22*) closed-cycle refrigerator from *CTI Cryogenics*; luminescence spectra were corrected for the instrumental function, but not excitation spectra; lifetimes are averages of at least 3–5 independent determinations; ligand excitation and emission spectra were recorded on a *Perkin-Elmer-LS-50* spectrometer equipped for low-temperature measurements.

REFERENCES

[1] J.-M. Lehn, *Angew. Chem. Int. Ed.* **1990,** *29,* 1304; V. Balzani, *Tetrahedron* **1992,** *48,* 10443; P.L. Anelli, P.R. Ashton, R. Ballardini, V. Balzani, M. Delgado, M.T. Gandolfi, T.T. Goodnow, A.E. Kaifer, D. Philip, M. Pietraszkiewicz, L. Prodi, M.V. Reddington, A.M.Z. Slavin, N. Spencer, J.F. Stoddart, C. Vincent, D.J. Williams, *J. Am. Chem. Soc.* **1992,** *114,* 193.

[2] J.-C. Chambron, V. Heitz, J.-P. Sauvage, *J. Am. Chem. Soc.* **1993,** *115,* 12378.

[3] J.-P. Sauvage, J.-P. Collin, J.-C. Chambron, S. Guillerez, C. Coudret, V. Balzani, F. Barigelletti, L. De Cola, L. Flamigni, *Chem. Rev.* **1994,** *94,* 993.

[4] J.-C.G. Bünzli, P. Froidevaux, J. Mac B. Harrowfield, *Inorg. Chem.* **1993,** *32,* 3306; P. Guerriero, P.A. Vigato, J.-C.G. Bünzli, E. Moret, *J. Chem. Soc., Dalton Trans.* **1990,** 647; G. Denti, S. Serroni, S. Campagna, A. Juris, M. Ciano, V. Balzani, in 'Perspectives in Coordination Chemistry', Eds. A.F. Williams, C. Floriani, and A.E. Merbach, VHCA, Basel, 1992, p. 153; N. Sabbatini, M. Guardigli, J.-M. Lehn, *Coord. Chem. Rev.* **1993,** *123,* 201; Z. Pikramenou, Y. Yu, R.B. Lessard, A. Ponce, P.A. Wong, D.G. Nocera, *Coord. Chem. Rev.* **1994,** *132,* 181.

[5] C. Piguet, J.-C. G. Bünzli, G. Bernardinelli, G. Hopfgartner, A.F. Williams, *J. Am. Chem. Soc.* **1993,** *115,* 8197.

[6] A. Juris, V. Balzani, S. Campagna, G. Denti, S. Serroni, G. Frei, H.U. Güdel, *Inorg. Chem.* **1994,** *33,* 1491.

[7] C. Fraser, R. Ostrander, A. L. Rheingold, C. White, B. Bosnich, *Inorg. Chem.* **1994,** *33,* 324; H. Okawa, J. Nishio, M. Ohba, M. Tadokoro, N. Matsumoto, M. Koikawa, S. Kida, D.E. Fenton, *ibid.* **1993,** *32,* 2949.

[8] P.V.N. Baxter, J.-M. Lehn, J. Fischer, M.-T. Youinou, *Angew. Chem. Int. Ed.* **1994,** *33,* 2284; E.C. Constable, *Tetrahedron* **1992,** *48,* 10013.

[9] C. Piguet, G. Bernardinelli, B. Bocquet, A. Quattropani, A.F. Williams, *J. Am. Chem. Soc.* **1992,** *114,* 7440.

[10] R. Krämer, J.-M. Lehn, A. Marquis-Rigault, *Proc. Natl. Acad. Sci. U.S.A.* **1993,** *90,* 5394.

[11] C. Piguet, B. Bocquet, G. Hopfgartner, *Helv. Chim. Acta* **1994,** *77,* 931.

[12] C. Piguet, G. Bernardinelli, A.F. Williams, B. Bocquet, *Angew. Chem. Int. Ed.* **1995,** *34,* 582.

[13] C. Piguet, G. Hopfgartner, B. Bocquet, O. Schaad, A.F. Williams, *J. Am. Chem. Soc.* **1994,** *116,* 9092.

[14] C. Piguet, G. Bernardinelli, B. Bocquet, O. Schaad, A.F. Williams, *Inorg. Chem.* **1994,** *33,* 4112; L.J. Charbonnière, G. Bernardinelli, C. Piguet, A.M. Sargeson, A.F. Williams, *J. Chem. Soc., Chem. Commun.* **1994,** 1419.

[15] C. Piguet, G. Hopfgartner, A.F. Williams, J.-C.G. Bünzli, *J. Chem. Soc., Chem. Commun.* **1995,** 491.

[16] C.G. Bochet, C. Piguet, A.F. Williams, *Helv. Chim. Acta* **1992,** *75,* 1697.

[17] C. Piguet, J.-C.G. Bünzli, G. Bernardinelli, C.G. Bochet, P. Froidevaux, *J. Chem. Soc., Dalton Trans.* **1995,** 83.

[18] G. Hopfgartner, C. Piguet, J.D. Henion, A.F. Williams, *Helv. Chim. Acta* **1993,** *76,* 1759.

[19] G. Hopfgartner, C. Piguet, J.D. Henion, *J. Am. Soc. Mass Spectrom.* **1994,** *5,* 748.

[20] E. Leize, A. Vandorsselaer, R. Krämer, J.-M. Lehn, *J. Chem. Soc., Chem. Commun.* **1993,** 990.

[21] C. Piguet, B. Bocquet, E. Müller, A.F. Williams, *Helv. Chim. Acta* **1989,** *72,* 323.

[22] E.R. Malinowski, D.G. Howery, 'Factor Analysis in Chemistry', Wiley, New York, 1980.

[23] E.C. Constable, S. Elder, J.V. Walker, P.P. Wood, D.A. Tocher, *J. Chem. Soc., Chem. Commun.* **1992,** 229.

[24] D.K. Lavalle, M.D. Baugham, M.P. Phillips, *J. Am. Chem. Soc.* **1977,** *99,* 718.

[25] J.H. Forsberg, *Coord. Chem. Rev.* **1973,** *10,* 195; R.C. Grandly, T. Moeller, *J. Inorg. Nucl. Chem.* **1970,** *32,* 333; M. Frechette, I.R. Butler, R. Hynes, C. Detellier, *Inorg. Chem.* **1992,** *31,* 1650; N. Sabbatini, M. Guardigli, I. Manet, R. Ungaro, A. Casnati, C. Fischer, R. Ziessel, G. Ulrich, *New. J. Chem.* **1995,** *19,* 137.

[26] G. Bernardinelli, C. Piguet, A.F. Williams, *Angew. Chem. Int. Ed.* **1992,** *12,* 1622.

[27] J.-C.G. Bünzli, V. Kasparek, *Inorg. Chim. Acta* **1991,** *182,* 101; J.-C.G. Bünzli, J.-P. Metabanzoulou, P. Froidevaux, L. Jin, *Inorg. Chem.* **1990,** *29,* 3875.

[28] B.M. Alsaadi, F.J.C. Rassotti, R.J.P. Williams, *J. Chem. Soc., Dalton Trans.* **1980,** 2147.

[29] I. Bertini, C. Luchinat, 'NMR of Paramagnetic Molecules in Biological Systems', Benjamin/Cummings Publishing Co., Inc., 1986, Chapt. 10.

[30] S. Rüttimann, C. Piguet, G. Bernardinelli, B. Bocquet, A.F. Williams, *J. Am. Chem. Soc.* **1992,** *114,* 4230.

[31] H. Friebolin, 'Basic One and Two-dimensional NMR Spectroscopy', VCH, Weinheim, 1991, p. 251.

[32] C. Piguet, J.-C.G. Bünzli, G. Bernardinelli, A.F. Williams, *Inorg. Chem.* **1993,** *32,* 4139.

[33] G.R. Choppin, in 'Lanthanide Probes in Life, Chemical and Earth Sciences', Eds. J.-C.G. Bünzli and G.R. Choppin, Elsevier, Amsterdam, 1989, Chapt. 1.

[34] C.N. Reilley, B.W. Good, J.F. Desreux, *Anal. Chem.* **1975,** *47,* 2111.

[35] J. Lisowski, J.L. Sessler, V. Lynch, T.D. Mody, *J. Am. Chem. Soc.* **1995,** *117,* 2273.

[36] R. M. Golding, M. P. Halton, *Aust. J. Chem.* **1972,** *25,* 2577.
[37] B. Bleaney, *J. Magn. Reson.* **1972,** *8,* 91.
[38] S. T. Frey, W. DeW. Horrocks, *Inorg. Chim. Acta* **1995,** *229,* 383.
[39] M. R. Wilcott, R. E. Lenkinski, R. E. Davis, *J. Am. Chem. Soc.* **1972,** *94,* 1742.
[40] A. D. Sherry, C. A. Stark, J. R. Ascenso, C. F. G. C. Geraldes, *J. Chem. Soc., Dalton Trans.* **1981,** 2078.
[41] I. Bertini, F. Capozzi, C. Luchinat, G. Nicastro, Z. Xia, *J. Phys. Chem.* **1993,** *97,* 6351.
[42] C. Piguet, A. F. Williams, G. Bernardinelli, E. Moret, J.-C.G. Bünzli, *Helv. Chim. Acta* **1992,** *75,* 1697.
[43] J.-C.G. Bünzli, in 'Lanthanide Probes in Life, Chemical and Earth Sciences', Eds. J.-C.G. Bünzli and G. R. Choppin, Elsevier, Amsterdam, 1989, Chapt. 7.
[44] J.-C.G. Bünzli, G. O. Pradervand, *J. Chem. Phys.* **1986,** *85,* 2489; J.-C.G. Bünzli, D. Plancherel, G. O. Pradervand, *J. Phys. Chem.* **1989,** *93,* 980; D. Plancherel, L. Jin, R. Massara, J.-C.G. Bünzli, *Helv. Chim. Acta* **1987,** *70,* 1298; F. Nicolo, D. Plancherel, G. Chapuis, J.-C.G. Bünzli, *Inorg. Chem.* **1988,** *27,* 3518.
[45] J. S. Lindsey, *New. J. Chem.* **1991,** *15,* 153.
[46] J. F. Desreux, in 'Lanthanide Probes in Life, Chemical and Earth Sciences', Eds. J.-C.G. Bünzli, and G. R. Choppin, Elsevier, Amsterdam, 1989, Chapt. 2., p. 43.
[47] W. C. Wolsey, *J. Chem. Educ.* **1978,** *55,* A355.